S03120100-TRT10003
ORNL/TM-2022/2558

Oak Ridge National Laboratory Neutronics Analysis in Preparation of the Blue Room Experiment

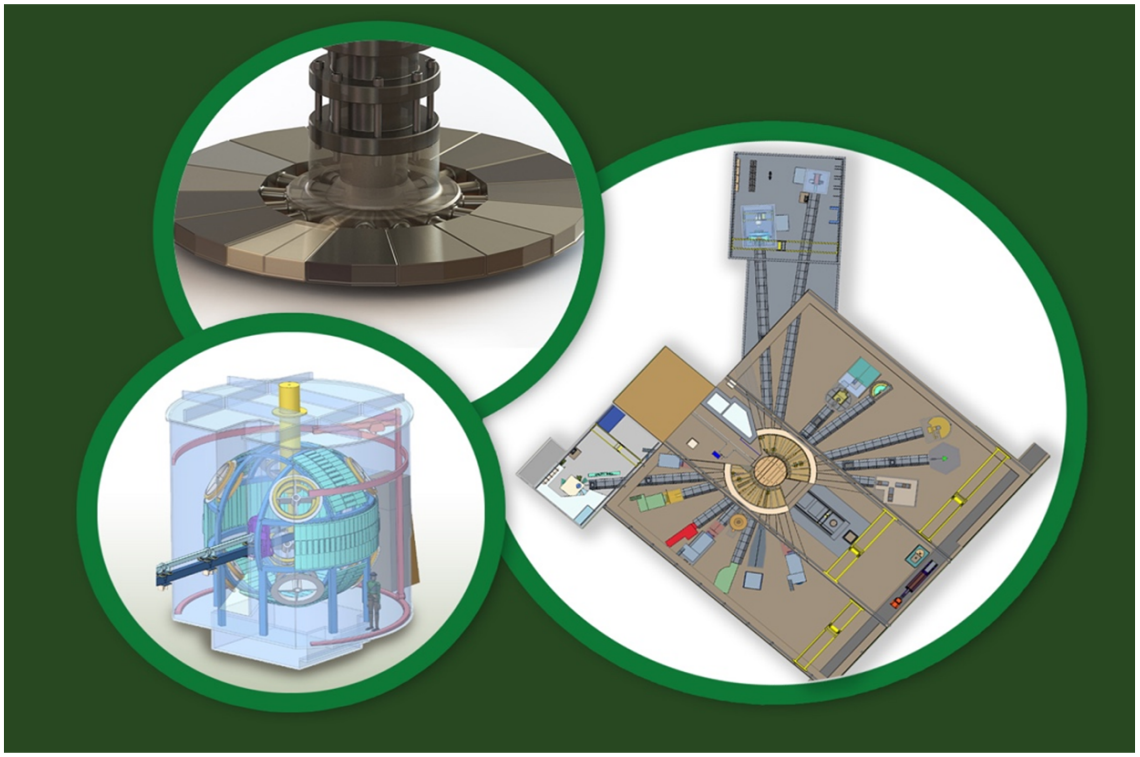

Kristel Ghoos
Igor Remec

July 2022

Approved for public release.
Distribution is unlimited.

OAK RIDGE National Laboratory

ORNL IS MANAGED BY UT-BATTELLE LLC FOR THE US DEPARTMENT OF ENERGY

S03120100-TRT10003
ORNL/TM-2022/2558

Second Target Station Project

Neutronics Analysis in Preparation of the Blue Room Experiment

Kristel Ghoos
Igor Remec

July 2022

Prepared by
OAK RIDGE NATIONAL LABORATORY
Oak Ridge, TN 37831
managed by
UT-Battelle LLC
for the
US DEPARTMENT OF ENERGY
under contract DE-AC05-00OR22725

CALCULATION TITLE

Neutronics Analysis in Preparation of the Blue Room Experiment

LABORATORY ORNL	DIVISION/GROUP Second Target Station (STS) Project	CALC NO. S03120100-TRT10003
Prepared by Kristel Ghoos	Level III Manager Igor Remec	Lead Engineer Justin Mach
Other WBS elements affected S031201		

Signature/Date

	REV 0	REV 1	REV 2	REV 3
Prepared By	Kristel Ghoos Digitally signed by Kristel Ghoos Date: 2022.08.17 16:29:38 -04'00'			
Task Leader	Kristel Ghoos Digitally signed by Kristel Ghoos Date: 2022.08.17 16:29:58 -04'00'			
Level III Manager	Igor Remec Digitally signed by Igor Remec Date: 2022.08.17 17:33:59 -04'00'			
Checked By	Tucker McClanahan Digitally signed by Tucker McClanahan Date: 2022.08.18 08:44:27 -04'00'			
Lead Engineer	Justin Mach Digitally signed by Justin Mach Date: 2022.08.30 21:32:23 -04'00'			

CONTENTS

LIST OF FIGURES

LIST OF TABLES

ABBREVIATIONS

ORNL	Oak Ridge National Laboratory
SNS	Spallation Neutron Source
STS	Second Target Station

EXECUTIVE SUMMARY

The goal of the Blue Room experiment is to investigate the 'thermal shock' stress in a tungsten target provoked by proton pulse impact. Short, strong pulses of highly energetic protons cause a rapid energy deposition in tungsten, which leads to a sudden temperature rise. This thermal shock causes a stress response and leads to fatigue, which can limit the lifetime of the target. In the Blue Room experiment, tungsten blocks will be irradiated by pulses of 800 MeV protons with several intensities to gain understanding in the strain response of the tungsten block.

Accurate energy deposition profiles are essential to calculate the mechanical response of the target. Therefore, MCNP6 simulations have been performed for several tungsten block configurations and for several beam positions. The resulting energy deposition profiles have been made available for thermal stress analysis. The initial design of 25 cm long tungsten block has been shortened to 22 cm to avoid the small peak and sudden drop in the energy deposition related to the Bragg peak, which happens just before the protons come to rest.

After the experiment, the tungsten is radioactive. Proton pulses create spallation and secondary particle interactions that activate the tungsten blocks. If there is a need to enter the room to remove the tungsten configuration shortly after the experiment (within ≈1 week), measures should be taken to limit exposure.

A 10-inch carbon steel shielding on all sides of the tungsten is needed to reduce the dose rates after the irradiation. This shielding efficiently reduces the radiation field from the activated tungsten but becomes highly activated itself if it is present during the experiment. The dominant gamma-emitter for short decay times (≈1 hour) is Mn-56, produced by interaction of a highly energetic neutron with Fe-56, one of the major isotopes in carbon steel. Because of the 2.5-hour half-life, dose rates drop significantly after 8 hours to 1 day.

To reduce radiation exposure from activation as much as possible after the experiment, additional shielding can be placed in the room after the experiment. Significant reductions in dose rates can be obtained by using a lead blanket over the tungsten/steel configuration or by adding a lead brick wall in the room.

The neutrons and protons escaping the tungsten blocks can be used to irradiate potential materials for the Target Viewing Periscope (TVP) windows to evaluate them for irradiation damage. Although most of the energy deposition in this experiment comes from ionization paths of protons, rather than from interaction with low-energy neutrons (as is the case in the TVP), the results could give a first indication and help in deciding further investigations.

The total energy deposition in the windows can be increased by using additional proton pulses (after the tungsten experiment) directly impinging on the windows. However, this will also cause significantly higher activation of the tungsten-steel configuration. A similar window material experiment could be performed at a proton irradiation facility such as ProNova[1], at which the same energy deposition can be accumulated within an hour.

It was estimated that 1 to 3 months cooling time will be necessary for the residual dose rate to decrease to ≈10 mrem/h which allows hands-on investigation of the radiation damage in the window material samples.

1 SCOPE

The primary goal of the experiment planned at the LANSCE Weapons Neutron Research (WNR) Target 2 (Blue Room) is to understand the 'thermal shock' stress due to a rapid energy deposition and subsequent temperature rise in a tungsten block following a proton beam pulse impact. A secondary goal of the experiment is to gain knowledge in the irradiation damage in candidate materials for the target viewing periscope window.

The objectives of this neutronics analysis are to support the preparation of this experiment by providing

1. the energy deposition in the tungsten block,
2. the activation dose rates from the tungsten block after the experiment,
3. mitigation solutions to limit radiation exposure after the experiment,
4. the energy deposition in windows,
5. the activation dose rates from the windows.

This work includes the response to Neutronics Task Order 3 (S.07.03.2021-01-05 LANSCE ENERGY DEPOSITION).

2 ASSUMPTIONS AND LIMITATIONS

This analysis is providing results necessary to plan and prepare the tungsten irradiation experiment in the Blue Room. Specific assumptions and limitations in the modeling are explained in the methodology and models section for each case. The analyses were performed with the methods and codes that are routinely used for the second target design. However, the predicted residual dose rates should be used with a healthy amount of conservatism following the established experimental procedures and adhering with ALARA requirements.

In this work, we intend to indicate the order-of-magnitude of magnitude of the activation dose rates to help planning a safe handling of the activated material. The results are not rigorous and should not be used for a Safety Basis. Before personnel enters the room, measurements should be performed to assess the safety.

The following list gives an overview of some of the major assumptions:

- The room geometry has been mostly neglected. Most analysis focuses on the dose rates in close proximity of the tungsten, which are not expected to be highly affected by the room geometry.
- Information about any components in the room was unknown at the time of the analysis. Activation of these component might, however, contribute to the dose rates in the room.
- Nothing is known about the duration, timing, and location of the personnel that will be entering the room after irradation.
- The beam profile is based on preliminary information from LANL. The exact specifics of the beam are unknown and, therefore, the actual profile may deviate from what is used in this analysis.
- The actual pulse plan may be different from the planned one.
- The air density in this analysis assumes sea-level, while the facility is located at approximately 2 km altitude (which results in ≈25% lower density). As the beam in the simulations starts close to the tungsten (<1 m) and the analyzed dose rates are in close proximity to the tungsten, this assumption is not expected to have a large effect on the results. It is, however, not conservative.
- Considering a distributed activation source has a large influence on the dose rates, as we demonstrate in section 4.2.3. For most analysis in this work, the activation source has not been sufficiently segmented to capture these effects. These include the evaluation of the steel shielding and the cladding.
- In the calculations with activated steel shielding, the dose rates in the front of the configuration are underestimated as the activation of the shielding in front has not been considered.
- Mitigation strategies with a lead blanket and a lead wall have been evaluated. These are only intended as examples of actions to reduce dose rates using a quick evaluation. It should not be used to calculate reliable dose rates to personnel. No attempt was made to achieve a certain dose rate.
- The energy deposition in and the activation of the windows has been evaluated without the steel shielding. If the shielding is present, this will impact the results.

3 METHODOLOGY AND MODELS

3.1 TUNGSTEN ENERGY DEPOSITION ANALYSIS

The analyses use several configurations of tungsten blocks, as described in the following sections. Each new configuration involved an update to the latest configuration as it was planned for the experiment at the time.

3.1.1 Simple configuration

A 6 x 4.8 x 25 (W x H x L) cm pure tungsten block without cladding, surrounded by air, is irradiated by a single pulse proton beam with 3e13 protons with a proton energy of 800 MeV. The spatial profile of the pulse is approximated as a Gaussian:

$$p(x, \sigma) = \frac{1}{\sigma\sqrt{2\pi}} \exp\left(\frac{-x^2}{2\sigma^2}\right), \tag{1}$$

in both the x- and y- direction. Two beam profiles are considered: a nominal beam with σ=1 cm (FWHM = 2.35482 cm) in both the x- and y-direction, and a squeezed beam with σ=0.6 cm (FWHM =1.412892 cm) and σ=2.25 cm (FWHM =5.298345 cm) in respectively the x- and y-direction.

Tungsten (density 19.3 g/cm3) consists of 4 W-isotopes without impurities: W-182 (26.53%), W-183 (14.3%), W-184 (30.68%) and W-185 (28.46%). Air (density 0.00121 g/cm^3) consist of N-14 (78.4431%), O (21.0748%) and Ar (0.4671%). The composition of stainless steel 316 block (8 g/cm^3) is taken from ref [2], material 300. Tantalum (16.654 g/cm^3) is described as pure Ta-181. If available, tabular cross-sections are used. Above the transition energy of 150 MeV, nuclear models are used. Full details can be found in the MCNP input files saved on the archive drive (Appendix B).

A radiation transport analysis is performed using MCNP6.2 [3]. Tracked particles include protons, neutrons, photons, positive pions, neutral pions, deuterons, tritons, helions, and alpha particles. Cross-sections are used from ENDF7. If no cross-sections are available, enent generator models are used for elastic and nuclear interactions (in particular CEM for protons, neutrons, photons, positive pions, and ISABEL for deuterons, tritons, helions, alphas). Particle energies up to 900 MeV are considered. Proton energy is cut off at 1 keV The energy deposition is tallied using a TMESH tally for the total energy deposition.

Three layouts are considered (see figure 1 for a simple sketch):

- with the beam centered on the 6 x 4.8 cm face,
- with the center of the beam aimed in the middle of the 48mm edge (half of the beam does not hit the tungsten),
- with two tungsten blocks side by side (48 mm) with a 2 mm gap between and the proton beam centered in the middle of the gap.

For the simulations in section 3.3, a 25 cm stainless steel 316 block (8 g/cm3) is added behind the 25 cm tungsten block in the direction of the proton beam.

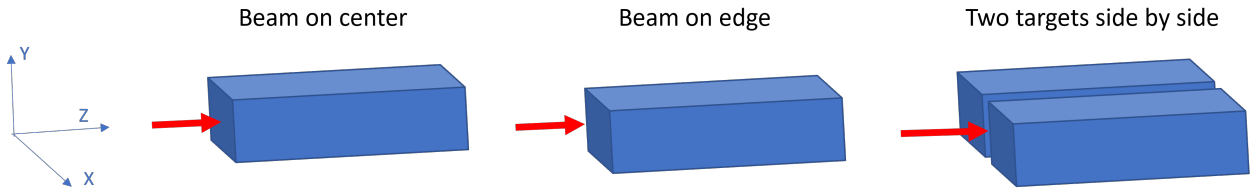

Figure 1. Sketch of the 3 block layouts.

3.1.2 Configuration with 3 blocks

This configuration consists of three tungsten blocks side by side with 2 mm gaps in between, see figure 2. Each block measures approximately 6cm x 4.8cm x 22cm, but a mild curvature around the z-axis and rounded edges in the front of the blocks are considered. One of the blocks has a 1 mm tantalum cladding all around.

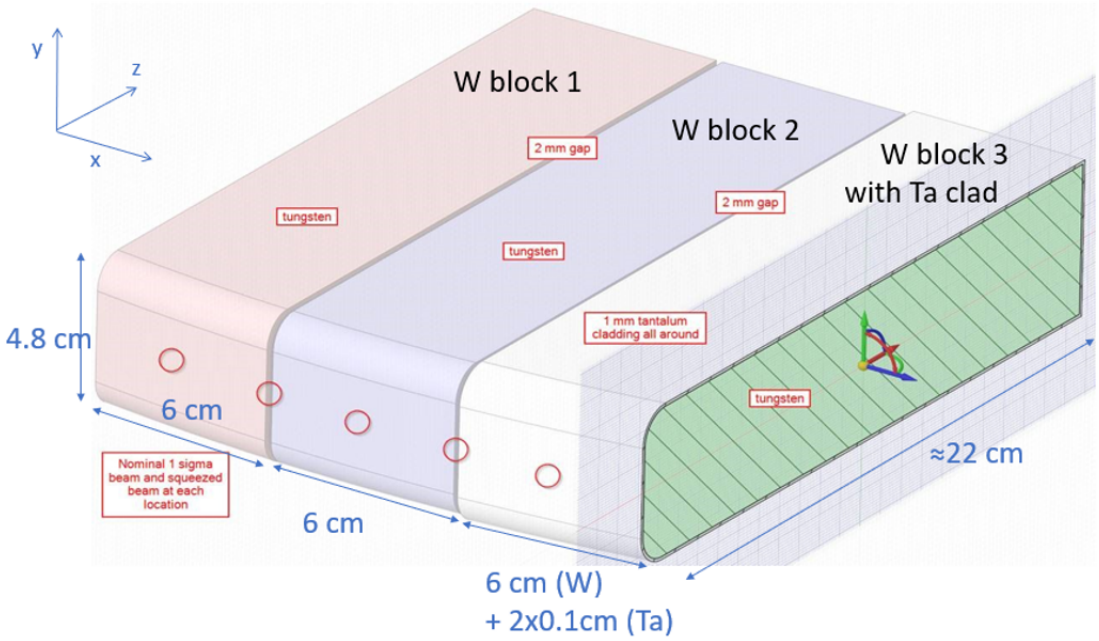

Figure 2. Schematic representation of the three block configuration.

To model this geometry with its curvatures in MCNP, we use an unstructured mesh constructed using Attila4MC. In the first few cm's in the front of the targets, a higher resolution mesh (2 mm maximum edge length) is used such that the energy deposition can be tallied with a sufficient resolution to be used for the thermal and stress analysis. To limit the total number of mesh-cells, a coarser resolution (5 mm maximum edge length) is chosen in the remainder of the blocks, where less energy is deposited. Curvature refinement is used to ensure sufficient resolution to capture the rounded edges.

3.1.3 Simplified 3-block configuration

The third configuration is a very similar but slightly simplified version of the model in figure 2. Each of the three tungsten blocks (no cladding) measures approximately 6 cm by 4.8 cm by 22 cm and and has rounded upper and lower front edges. There are 2 mm gaps between the blocks. Only one beam impact will be examined, directed towards the center of the middle tungsten block. It has a σ of 0.6 cm in both directions (this is smaller than the previously used nominal beam with a σ of 1 cm). The mesh, constructed with Attila4MC, has a higher resolution in the front part of the middle block, especially in the center of this block where the beam impacts (see figure 3). The maximum edge lengths are chosen as 1 mm (highest resolution at the center of the middle block), 2 mm (front part of the middle block), and 4 mm (block 1 and 3, rear part of block 2). This ensures sufficient detail for the stress analysis.

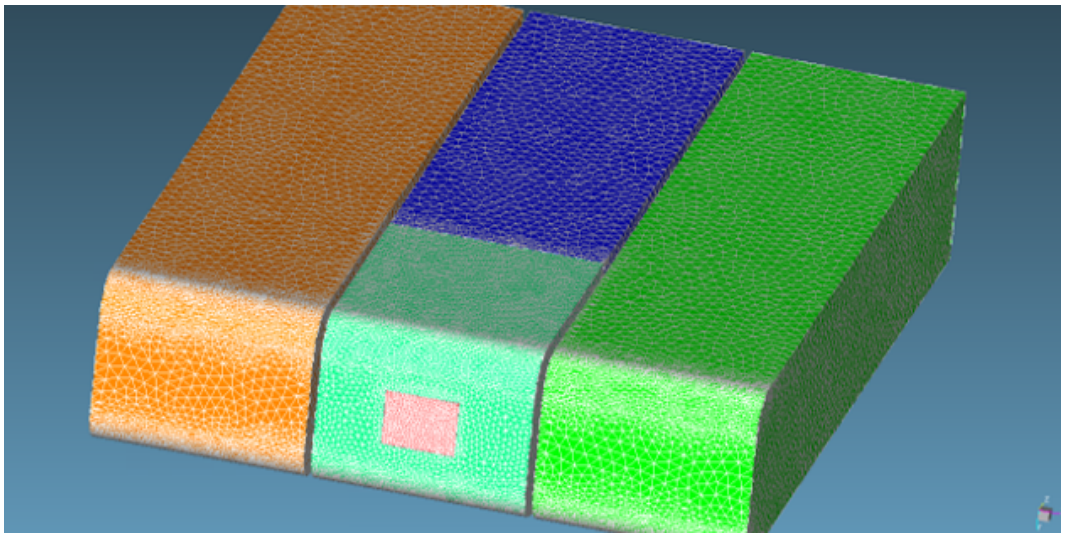

Figure 3. Mesh (constructed using Attila4MC) for the simplified 3-block geometry.

3.1.4 Simplified 3-block configuration with cladding

In the fourth configuration, a 1mm thick cladding is present on the third tungsten block. The energy deposition will be evaluated for two different cladding materials: tantalum (pure Ta181, 16.6 g/cc) and niobium (pure Nb93, 8.57 g/cc). Additionally, the energy deposition will be calculated for the configuration without cladding, in which the cladding material is replaced by air. A nominal beam with 1 cm sigma is directed towards the center of the third tungsten block. In figure 4, we show the meshed geometry constructed with Attila4MC. The maximum edge is 2 mm in the front part of block 3 (both the tungsten and cladding) and 5 mm in the rest of the geometry. Smaller mesh elements are used in the front of the third tungsten block to ensure sufficient resolution for stress analysis.

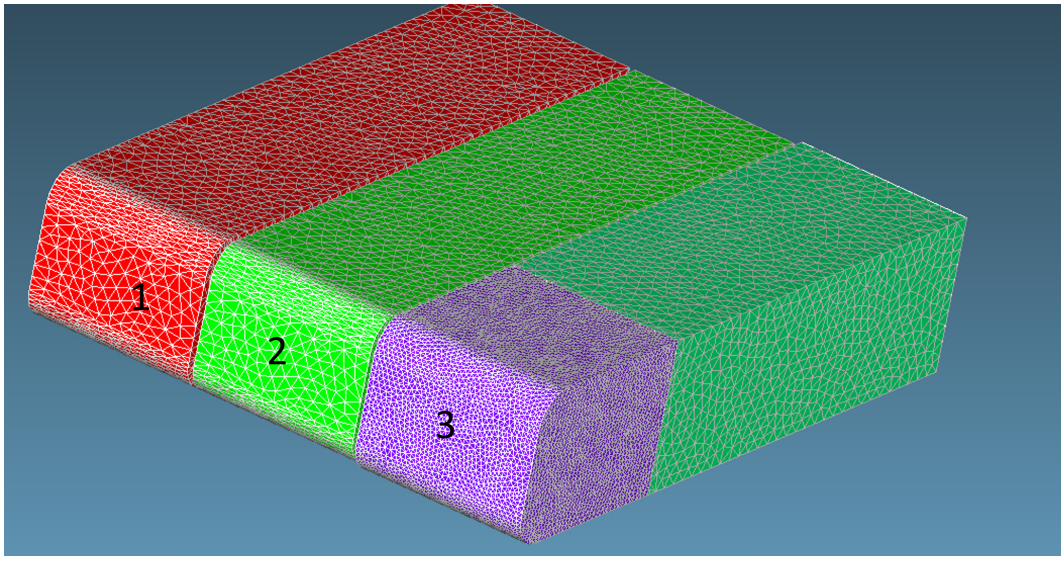

Figure 4. Mesh (constructed using Attila4MC) for the simplified 3-block geometry with cladding on the third block.

3.2 ACTIVATION CALCULATION

The residual gamma-ray dose rates due to activation are computed in three steps:

1. An MCNP transport calculation using the proton beam source resulting in neutron fluxes and spallation product generation rates.
2. CINDER activation calculations using the tallied neutron fluxes that determine the isotopic inventory and decay gamma-ray intensities.
3. An MCNP decay gamma transport calculation for the residual dose rates.

CINDER calculates the inventory of radioactive and stable nuclides over time and provides the corresponding gamma source definitions for MCNP. We use the version of CINDER2008 that is packaged with Activation in Accelerator Radiation Environments (AARE)[4, 5, 6]. As input, it requires the low-energy neutron fluxes (<20 MeV) and spallation product rates originating from high energy particles (>20 MeV). CINDER can only calculate the activation products from interaction with neutrons below 20 MeV, for which it has nuclear data available. The spallation products coming from particle interactions with higher energies are calculated based on nuclear models and tallied with the RNUCS tally in MCNP.

The flux-to-dose conversion factors(from gamma-flux to effective dose) are used from ICRP-74 up to 10 MeV extended up to 10 GeV [7]. A constant factor of 1.7466E-05 is assumed below 0.01 MeV to 0.001 MeV.

3.2.1 Activation of tungsten: simplified model

The input for this first MCNP calculation is very similar to the one described in the previous section, except for the tallies and the cross-sections. The neutron flux is tallied in several energy bins below 20 MeV, which is the range in which cross-section tables are used. For neutrons above 20 MeV, protons, and other

relevant particles (deuterons, tritons, helions, alphas), models are used and the RNUCS tally will score the activation products.

The three-block configuration is approximated by one tungsten block (the middle block from the three-block configuration in figure 2). The proton beam (gaussian) is directed towards the middle of the tungsten block (98% of the protons are hitting this tungsten block). As the two blocks on the sides receive only a few protons (<2%) but provide additional shielding, removing them from the configuration is a conservative approximation, in particular for the dose rates on the sides. The tungsten block is divided into 45 different MCNP-cells using a 3x3x5 mesh as shown in figure 5. With this 45-cell mesh, we approximate the non-uniform distribution of activation sources in the block. The dose rates resulting from this distributed source will be compared with those calculated with a single-cell Tungsten block for which the activation sources are uniformly distributed in the whole block.

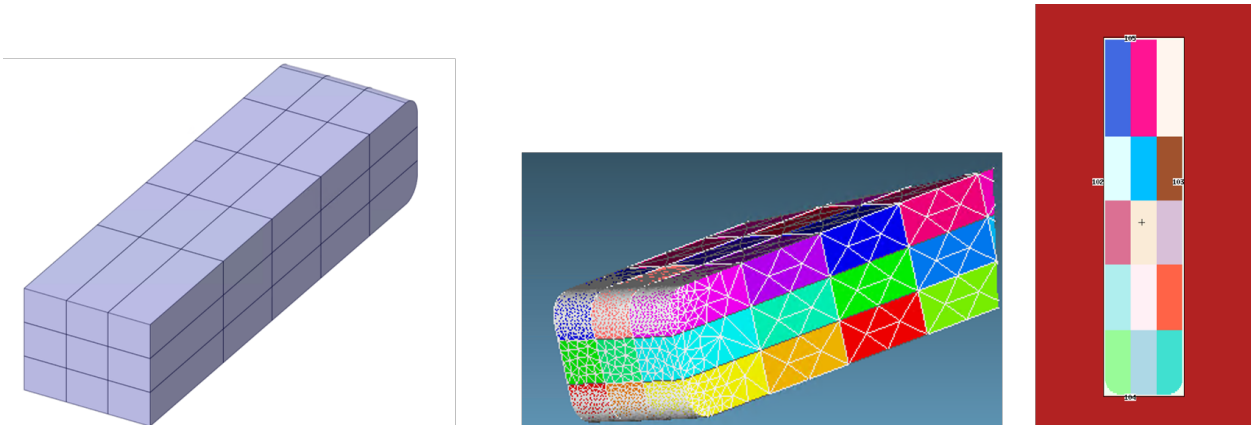

Figure 5. Tungsten block divided in 3x3x5 cells in SpaceClaim (left), the meshed geometry in Attila4MC (middle), and the y=0 plane view in the MCNP plotter (right)

This analysis assumes pure Tungsten without impurities. The effect of impurities is negligible: impurities with the guaranteed maximum values listed in [8] increase the activation sources by less than 1%.

Table 1 summarizes the pulse plan and the corresponding CINDER input parameters. Six irradiation series are planned, with a 3-hour break between the 3rd and 4th series. Irradiation starts with a proton pulse delivered to the center of the W block number one. Five pulses, one each 120 s, are delivered. After a 600 s pause, the beam is moved to the location between the first and second block and a sequence of 5 pulses is repeated. The beam position is repeatedly changed in equal steps until the center of the third block is reached. This completes the first irradiation series of 5 pulses delivered to each of the 5 locations. Two identical irradiation series follow with lower beam powers. After 3 hours break the irradiation resumes. The same five locations of the beam are used again, only now at each location 2 pulses are delivered (with 1/20 s inbetween the two pulses, 20 Hz) followed by 240 second pause and repeated 5 times; this completes the fourth irradiation series. Two identical additional series follow each with lower beam power. For the CINDER activation calculation, we approximate the pulsed history with a continuous irradiation history of the same total number of protons spread out over the total time of the considered interval. We consider a new time interval for each beam intensity change. An illustration of the irradiation history is

shown in figure 6. While in reality there will be 5 possible beam positions, the simplified model assumes a nominal beam impact (with σ=1 cm) centered on the front face of the tungsten block for all pulses.

Table 1. Approximate pulse plan and corresponding parameters for continuous irradiation for the activation calculation in CINDER. Full pulse strength = 3e13 protons (800 MeV) per pulse.

Relative pulse strength	Total number of pulses	Time per pulse [s]	Time to change set-up [s]	Averaged nr of protons/s in interval	Total time in interval
1	25	120	600 (5 times)	1.25e11	100 min
0.5	25	120	600 (5 times)	6.25e10	100 min
0.25	25	120	600 (5 times)	3.13e10	100 min
0	0	0	3 hr	0	3 hr
1	25x2	240/2	600 (5 times)	1.67e11	2.5 hr
0.5	25x2	240/2	600 (5 times)	8.33e10	2.5 hr
0.25	25x2	240/2	600 (5 times)	4.16e10	2.5 hr

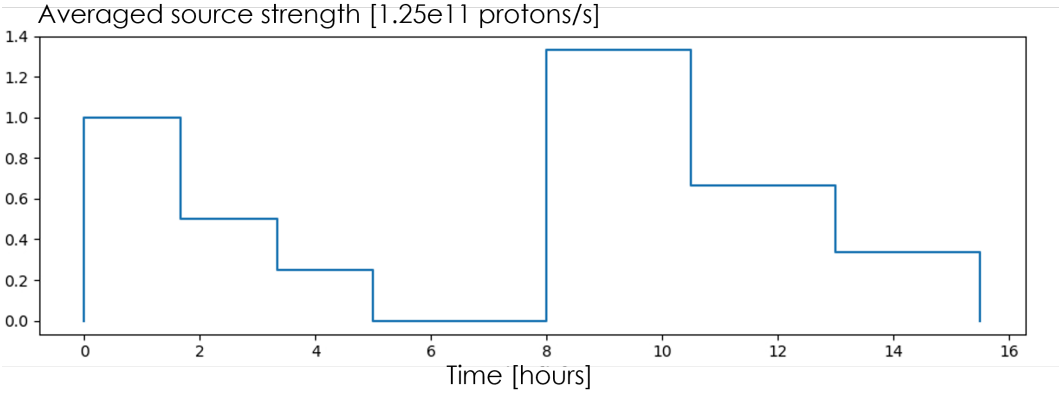

Figure 6. Average source strength as a function of time. This is used as a simplified irradiation history in CINDER.

The tungsten block is placed 1.5 m above the floor in a cylindrical, concrete room with 6.1 m radius and a 7.35 m height, see figure 7. Inside the room, there is also a rectangular beam stop (graphite) and a beam start (stainless steel). These dimensions are based on a simple technical drawing of the room and some available pictures. The target is positioned at the origin of the room geometry, ranging from x = -3 to 3 cm, y = -2.4 to 2.4, and z = 0 to 22 cm. Details of this geometry are of minor importance for the dose rates at 30 cm around the tungsten block: a simulation with and without the geometry result in «1% difference. The room geometry is not considered in the presented analysis.

Six detector tallies are placed at approximately 30 cm around this target. One in front with coordinates (x,y,z)=(0,0,-30), one in the back (0,0,52), one above the target (0,33,5.5), and on at the right side of the target (33,0,5.5).

Objects in the room can become activated and potentially provide a non-negligible dose. This has not been evaluated due to lack of knowledge of the objects in the room at the time of the analysis.

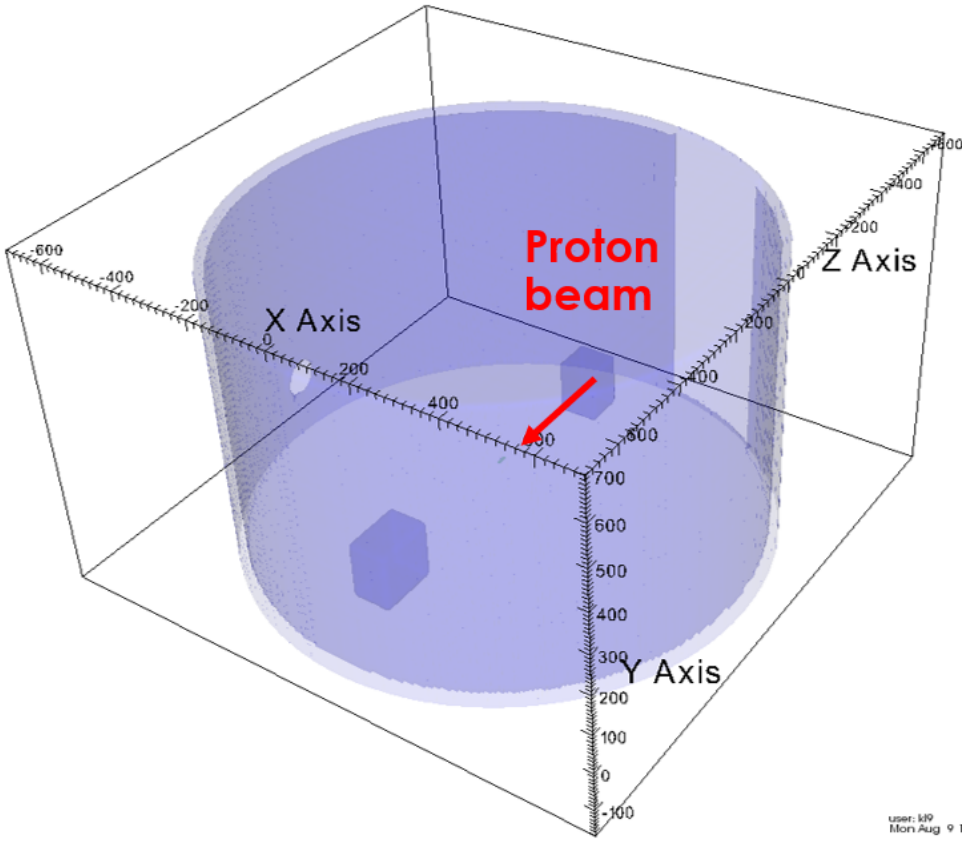

Figure 7. Tungsten block divided in 3x3x5 cells in SpaceClaim (left), the meshed geometry in Attila4MC (middle), and the y=0 plane view in the MCNP plotter (right)

3.2.2 Activation of tungsten: high-fidelity model

The most important differences with the simplified model are

- the geometry, which considers the three tungsten blocks (geometry of the room is ignored),
- the pulse history, in which each pulse is modeled separately.

The 3-block geometry of section 3.1.2 is used, but it is meshed differently. Like the meshing in the simplified activation model, each block is divided in 45 activation cells, which results in 135 activation cells for the three blocks. Within each block, Attila4MC is used to create a tetrahedral mesh that accurately captures the rounding in the geometry, see figure 8 .

We consider a detailed pulse history in which each pulse is modelled separately. The total pulse plan consists of 6 series, of which the first one is graphically represented in figure 9. This series is repeated for 2 lower beam intensities. Afterward, 3 more series with the 3 intensities are planned, in which each shot

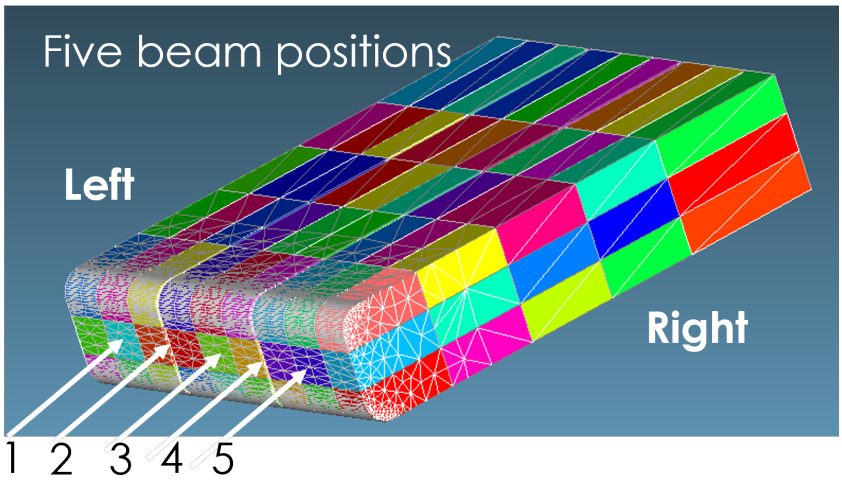

Figure 8. Meshed geometry in Attila4MC of the tungsten block configuration for the detailed analysis with the indication of the 5 beam positions

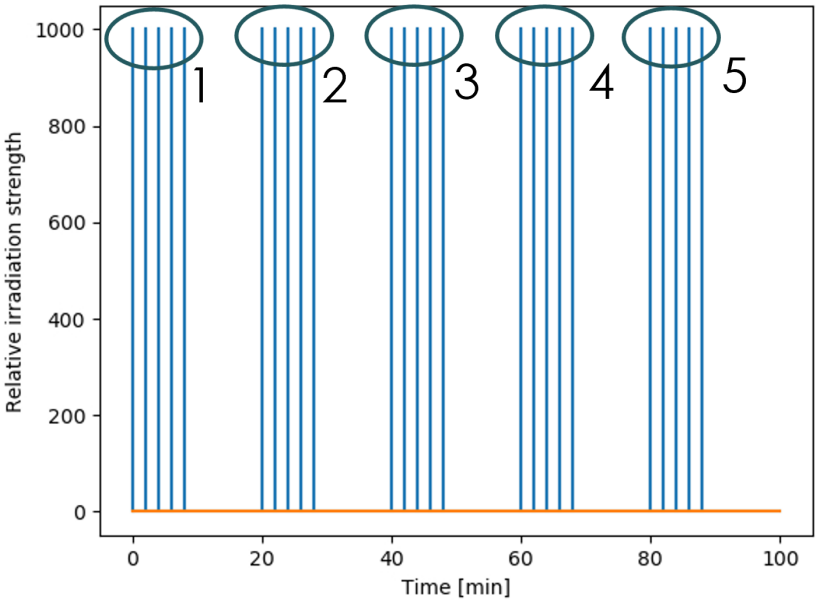

Figure 9. Representation of the first series of pulses, in which the beam position is changed every 5 pulses (the numbers indicate the beam position corresponding to figure 8) The orange line represents the level of the constant irradiation profile.

consists of 2 pulses at 20 Hz, with a 2 min break between shots. Beam positions progress from left (1) to right (5) in pulse series 1,3 and 5 and in the reverse order for series 2, 4 and 6. A pulse length of 1 ms has been used.

Two simulation approaches have been carried out. In the first approach, one activation run is performed separately for each of the 5 beam positions. The total source is constructed afterwards as the sum of the sources for the 5 positions. In the second approach the activation is performed for the first location of the

beam and the resulting isotopic content of the target is used as the starting point for the beam on the next location. This is more closely matching the actual conditions, however, both approaches give the same results: differences of only ≈0.01% are observed in the resulting activation source strengths.

3.2.3 Activation of steel shielding

As the shielding will be in place around the tungsten blocks during the experiment, the steel will become activated by the neutrons and the protons leaving the tungsten.

The geometry model for the activation calculations (see figure 10) consists of the three tungsten blocks, surrounded by 4-inch shielding on all sides except for the front, where protons enter. The activation of the front door (which will be further away in the room during the experiment) will be less than the activation on the other sides and is neglected. For the dose rate calculation, the front door is present (the dotted white lines in figure 10). The 4-inch steel box is divided into 10 cells to account for the distribution of the activation source: a higher amount of activation is expected in the inner layers of steel close to the tungsten than in the outer layers of steel. The steel on the sides is also distinguished from the steel in the back. The steel on the side makes no distinction between top/bottom and right/left. A higher dose is, however expected on top/bottom than on the right/left sides.

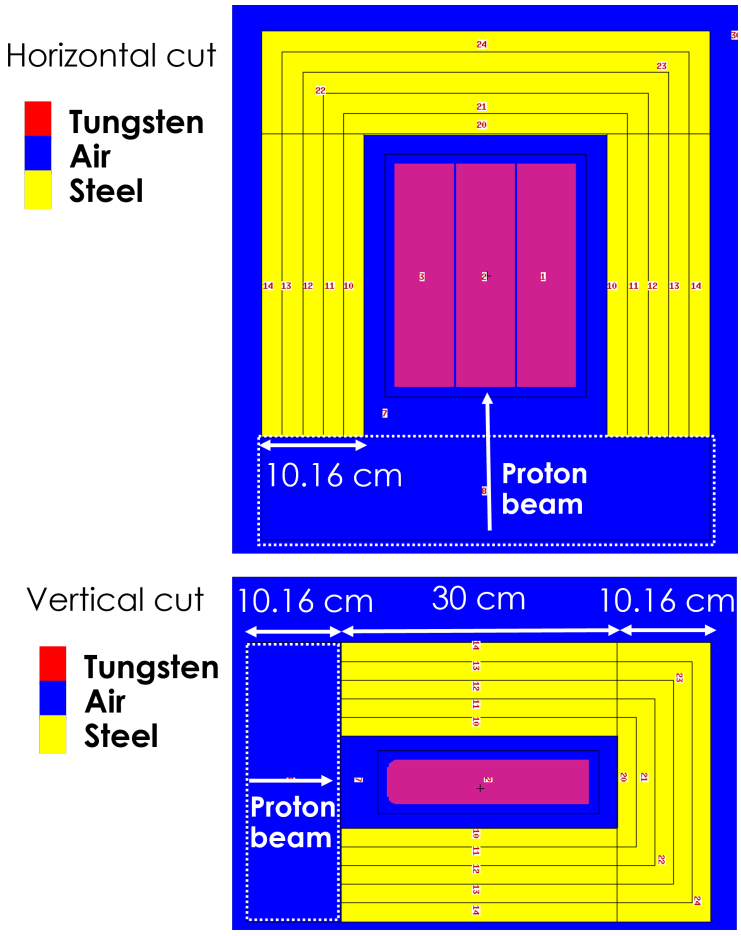

Figure 10. Geometry (MCNP) used for the activation analysis of the shielding

The source protons are equally distributed over the 5 beam positions with each a gaussian distribution (with σ= 1 cm). The x-coordinates of the positions are respectively -6.0305, -3.015, 0, 3.015, and 6.0305 cm. The irradiation history is simplified by the continuous irradiation profile of figure 6.

The steel shielding is modeled as pure carbon steel (see table 2). The impact of impurities is investigated by using two alternative compositions of steel (see table 2). The first alternative is steel 1020, taken from the STS database. The second alternative is steel A36 , for which we have taken the maximal amount of all impurities listed in the ASTM A36 chemical requirements. All steel is modeled with a density of 7.82 g/cc.

Table 2. Elemental composition with weight % pure carbon steel, steel 1020 (with a low level of impurities) and steel A36 (with a high level of impurities). We assume a density of 7.82 g/cc for all.

	Carbon steel (no impurity)	**Steel 1020** (low impurity)	**Steel A36 (high impurity)**
C	5	0.2	0.28
Si	0	0.25	0.4
P	0	0	0.4
S	0	0	0.5
Mn	0	0.45	0.9
Fe	95	99.1	97.32
Cu	0	0	0.2

Table 3. Elemental composition of Al6061 with a high level of impurities. We assume a density of 2.7 g/cc.

Element	**Weight %**
Mg	1.2
Al	96.4
Si	0.4
Ti	0.15
Mn	0.15
Fe	0.7
Cu	0.4
Zn	0.25

Tungsten and air have the same composition as described before in section 3.1.1. Lead is modeled as pure lead without impurities and a density of 11.35 g/cm3. For aluminum, the material description of Al6061 is taken from the STS database. To examine the potential effect of impurities in a conservative manner, a high-impurity material description is sometimes used which takes the maximal chemical composition limits for each impurity element as listed by the B247M-20 standard for Al6061-T6 (see table 3).

After irradiation the front shielding will be put in place, and it is, therefore, included in the geometry model for the dose rate calculations. Detector tallies are placed at 30 cm from the front, left, top and back of the steel shielding, with coordinates (x,y,z) of respectively (0,0,-45.16), (-52.16,0,11), (0,45.16,11) and (0,0,65.16). As the activation of the front shield is neglected, the calculated dose rates in front of the steel

shielding will be underestimated. Results for this front detector will either not be mentioned or will be indicated with an asterisk * to remind the reader that these values are underestimated.

To mitigate high dose rates, it is considered to use a lead blanket after irradiation. The calculation assumes a 1.27 cm (0.5 in) layer of lead with a density of 4.8055 g/cc at all sides of the shielding (left, right, top, bottom, front and back).

To provide additional shielding for people entering the room after irradiation, a wall of lead bricks can be built. There are 46 lead bricks available, each measuring 8”x4”x2”. As an example, we assume a wall consisting of 5x8 bricks, which results in a horizontal and vertical length of respectively 101.6 cm and 81.28 cm. The 5.08 cm thick wall is placed approximately 30 cm from the steel shielding at one side. Figure 11 shows a horizontal and vertical cut of this geometry in MCNP. As the room geometry has not been taken into account, the impact of scattered particles from the room walls has not been evaluated.

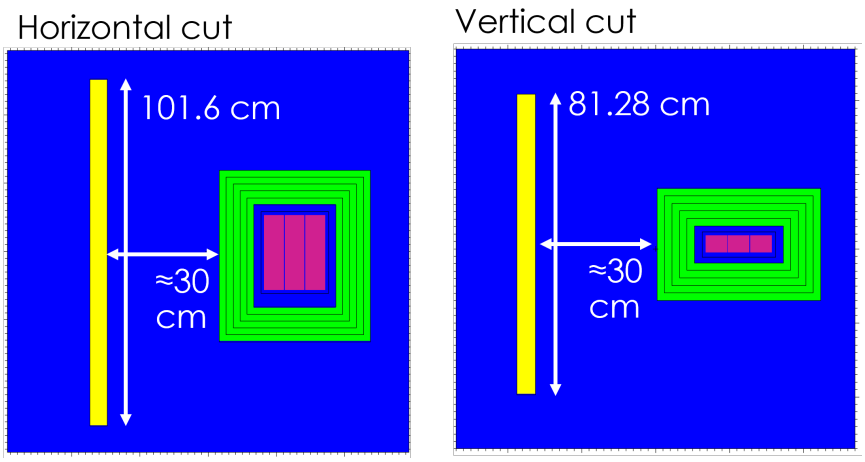

Figure 11. Positioning of the lead wall (yellow) to the side of the tungsten blocks (magenta) surrounded by steel (green).

3.2.4 Activation of cladding material

For this calculation, the simplified 3-block configuration has been adapted to have a 1 mm thick cladding on the right block. The simplified continuous irradiation history is used. The source protons are equally distributed over the 5 beam positions with each a gaussian distribution (with σ= 1 cm). Attila4MC has been used to construct an unstructured mesh for MCNP. A simple activation mesh is used: each tungsten block is modeled as 1 activation cell, the cladding as a whole is 1 activation cell.

Two cladding materials are considered: tantalum, which is described as Ta-181 with a density of 16.6 g/cm3 (the small fraction of Ta180 is omitted), and niobium, which is described as pure Nb-93 with a density of 8.57 g/cm3.

Detectors are placed 30 cm from the front, back, top, and left and right sides of the tungsten blocks. Comparing dose rates at the left and right detectors, the influence of the cladding material can easily be assessed. This is not a rigorous analysis, but it will give an indication of whether the cladding material will impact the dose rates drastically or not.

3.3 WINDOW IRRADIATION

The protons and neutrons emitted from the tungsten blocks during the experiment can be used to irradiate potential window materials. In this section, we describe the model and calculation details for the energy deposition and activation analysis. These calculations do not consider the steel shielding unless otherwise stated.

3.3.1 Energy deposition

To evaluate the total dose that the windows receive during the experiment (16.2 hours), we assume an average proton irradiation of the tungsten blocks of 6.7655e10 protons/s. This number is calculated by dividing the total number of protons launched towards the tungsten blocks (3.9375e15) by the duration of the experiment (16.2 hours). The protons are equally distributed over the 5 beam positions with each a gaussian distribution (with σ= 1 cm).

A window can be placed at 20 different locations: 10 windows are placed below the tungsten blocks, and 10 windows are placed on the sides and at the back. This way, there will be two locations for 10 different window materials. This can provide two different irradiation levels for each material. Figure 12 gives a representation of these window locations with snapshots from the CREO and MCNP model. In the MCNP model, the windows are modeled as disks (yellow) with a diameter of 2.5 cm and a variable thickness, depending on the material (see table 4). The tungsten blocks (magenta) are modeled as the 3-block configuration of section 3.1.3 using an unstructured mesh created using Attila4MC. The windows and tungsten blocks are surrounded by air (blue). The material description of air and tungsten are the same as in previous cases. The materials currently considered for the window, with their density and thickness, are listed in table 4. All these materials are modeled without impurities.

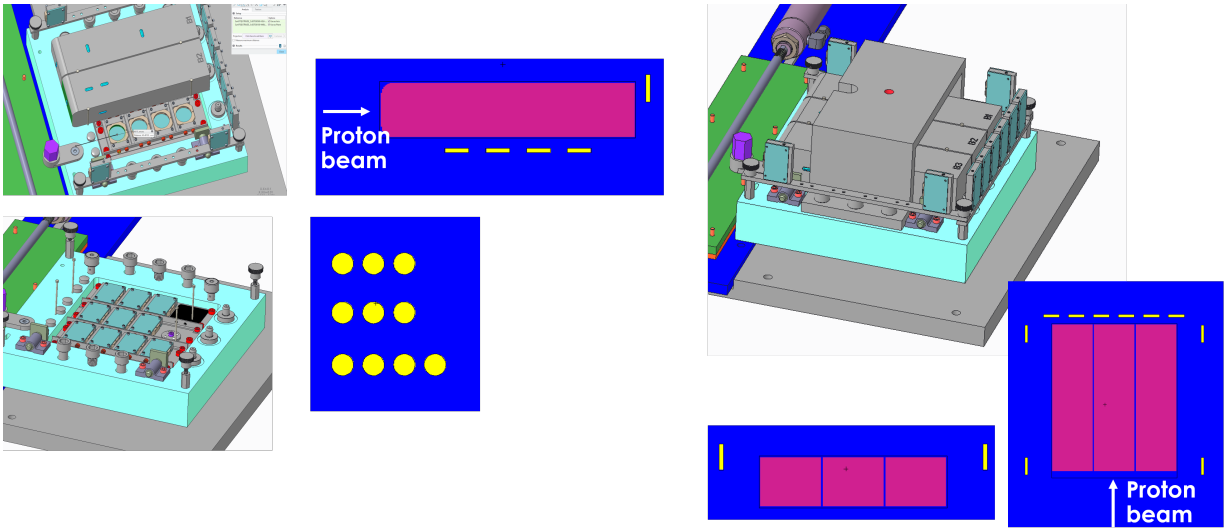

Figure 12. Snap shots to give an impression of the window locations in CREO and MCNP.

Table 4. Density and thickness for each window material

	BaF2	ZnSe	ZnS	CaF2	Ge	MgF2	Sapphire (Al2O3)	Quartz (SiO2)	Fused Si (SiO3)
Density [g/cc]	4.89	5.27	4.08	3.18	5.33	3.18	3.97	2.649	2.203
Thickness [mm]	4	4	4	4	4	4	5	2.6	3

The energy deposition is tallied using F6 tallies: F6:n, F6:h and F6:p for separate contributions of the neutrons, protons and photons respectively, and +F6 for the total energy deposition from all tracked particles (neutrons, photons, pions (positive, negative and neutral), muons (positive and negative), kaons (positive, negative, short, long), deuterons, tritons, helions, alpha particles). The contribution of electrons is taken into account using the thick bremsstrahlung approximation in photon transport. Considering the small thickness of the disks, this can result in a slight overestimation. For a few simulations, in which the relative electron contribution (F6:e) is high, electrons are tracked to increase the accuracy.

3.3.2 Activation: window at a high neutron irradiation location

To examine the windows after the experiment (for which hands-on handling is required), the dose rates from activation need to be sufficiently low within a reasonable decay time.

The simplified window model consists of the window itself (here BaF2, indicated in white, 5mm thick) and is surrounded by a casing. The materials of this casing (including the screws) consist of Al6061 and S304 components (1.5 cm thick). The geometry has been simplified as shown in figure 13. Material description for S304 (8.0 g/cc) is taken from [2]. To have a conservative estimate of the dose rates, the window model is placed at a high neutron irradiation location, chosen based on the neutron dose rate maps.

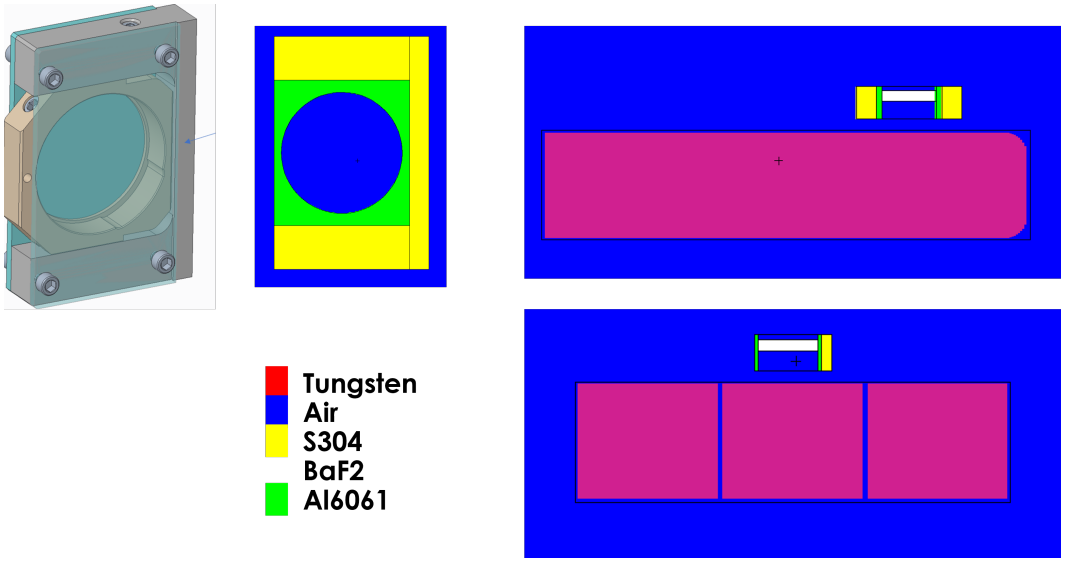

Figure 13. MCNP model to calculate the activation of the window materials

3.3.3 Activation: additional pulses in front of the shielded tungsten blocks

It is considered to place a window immediately in front of the proton beam to be able to reach a higher energy deposition in the window material. After the tungsten experiment has finished, the front steel shielding will be placed in front of the tungsten blocks such that the tungsten configuration is fully surrounded by steel. Four window materials (e.g., BaF2, ZnS, ZnSe, CaF2) can be attached at the outside of this shielding door such that they can be irradiated by the next proton pulses. These proton pulses will be additional to the original irradiation plan, and are, therefore, not considered in the activation calculation so far. In these calculations, we need to evaluate both the activation of the tungsten and steel configuration and of the window itself.

To calculate the activation of the tungsten configuration, steel shielding and window materials from these additional pulses, the MCNP model is shown in figure 14. This model adds two components to tungsten and steel configuration in figure 10. First, the front shielding door is present, as the rest of the shielding it is divided into 5 different cells to account for the distribution of the activated materials. Second, a window with casing is placed in front of the shielding. For dose calculation afterwards, we examine both the whole model, and separately the window and its frame.

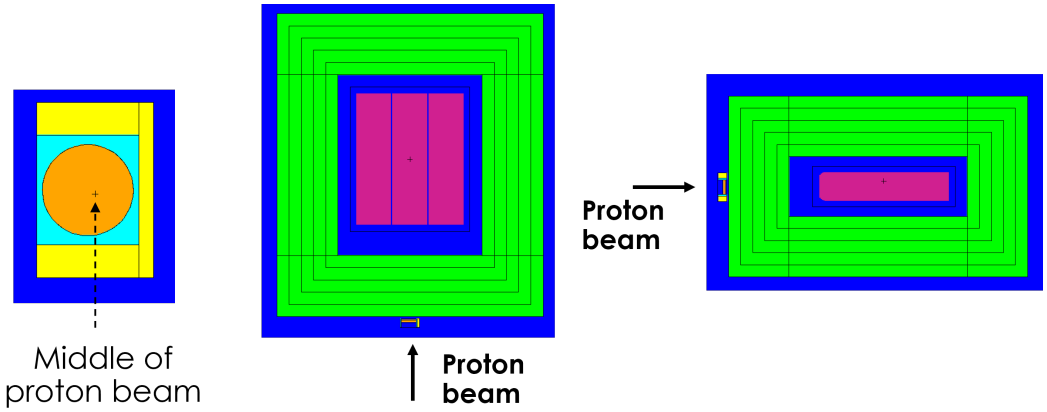

Figure 14. MCNP model to calculate the activation from additional pulses

4 ANALYSIS AND RESULTS

4.1 ENERGY DEPOSITION

4.1.1 Energy deposition for the three simple configurations

A summary of the total energy deposition for the three layouts is listed in table 5. In Appendix C, a few cuts in the geometry with the local values are shown. Peak values inside the tungsten block go up to approximately 30 J/cc. Most of the energy is deposited from protons (≈70%) and neutrons (≈20%), followed by photons (≈5%) and other particles (deuterons, alpha particles, neutral pions, tritons and helions, 5%).

When the beam is centered in the middle of the face of the tungsten block, almost all protons (98%) are incident on the block. Per incident proton (of 800 MeV) 445 MeV is deposited in the block on average. This results in an overall energy deposition of 2099 J per pulse. The rest of the energy (from incoming protons and the nuclear reactions) is transported in the secondary particles. When the proton beam is aimed at the edge, only half of the protons (49%) are incident on tungsten block. Moreover, less energy is deposited per proton (388 MeV) as more high-energy particles will escape from the face of the tungsten block parallel to the edge where the proton beam is aimed. This results in a much lower total energy deposition of 916 J.

When two tungsten blocks are placed side by side with a gap between them, with the proton beam aimed between the block, most protons are incident on the blocks (91%), however, around 8% are lost in the gap. Per proton, around 454 MeV is deposited on average, which is more than in the other layouts, because some of the particles escaping from one block can be captured by the other block, depositing energy there. In each block 988 J is deposited, which makes the total 1976 J for the two blocks.

In Figure 15, the total energy deposition is shown as a function of the z-direction (the proton beam direction) for the three layouts. The deposited energy density is integrated over the tungsten surface perpendicular to the beam.

After reaching its maximum value, which happens close to the front surface of the tungsten block, the energy deposition decreases until approximately z = 21 cm, where there is a sudden increase in energy deposition before decreasing to a negligible value after 22.7 cm. This peak is the so-called ‘Bragg peak’, in which there is an increased energy loss of protons traveling through matter just before they come to rest. A fast estimate of the location of this Bragg peak can be obtained using the Stopping and Range of Ions in Matter (SRIM) software [9]. For an 800 MeV proton beam in tungsten, a stopping range of 22.532 cm is predicted. This corresponds well with the MCNP results in which the energy deposition decreases to a negligible value after 22.7 cm. While this Bragg peak is low compared to the global peak in the beginning of the block, the sudden decrease to a negligible energy deposition might lead to unwanted effects in the stress response of the tungsten block. Simulations have been repeated with a block length of 22 cm for further stress analysis.

The differences between the energy deposition with the ‘beam on the edge’ and the ‘2 targets side by side’ lay-out are due to two effects. Close to the front surface of the tungsten block (z < 5 cm), the energy deposition is primarily from the primary proton beam and less energy is deposited when two targets are placed side by side, as many protons are flying through the gap without interacting with any of the targets. Further along the target (z > 5 cm), more energy is deposited when two targets are placed side by side. Here, deposited energy includes a significant contribution from secondary particles, and particles escaping

from one target can be captured by the other target, therefore more energy is deposited.

Table 5. Summary of total energy deposited for three considered layouts (total source strength = 3e13 protons)

Lay-out	Total energy deposited per pulse [J]	Peak energy deposition [J/cm3]	Number of protons incident on target	Percentage of protons hitting the target	Average energy deposition per incident proton [MeV]
Beam on center	2099	30	2.9428e13	98	445
Beam on edge	916	27	1.4738e13	49	388
Two targets side by side	1976 → 988 per target	29	2.71677e13	91	454

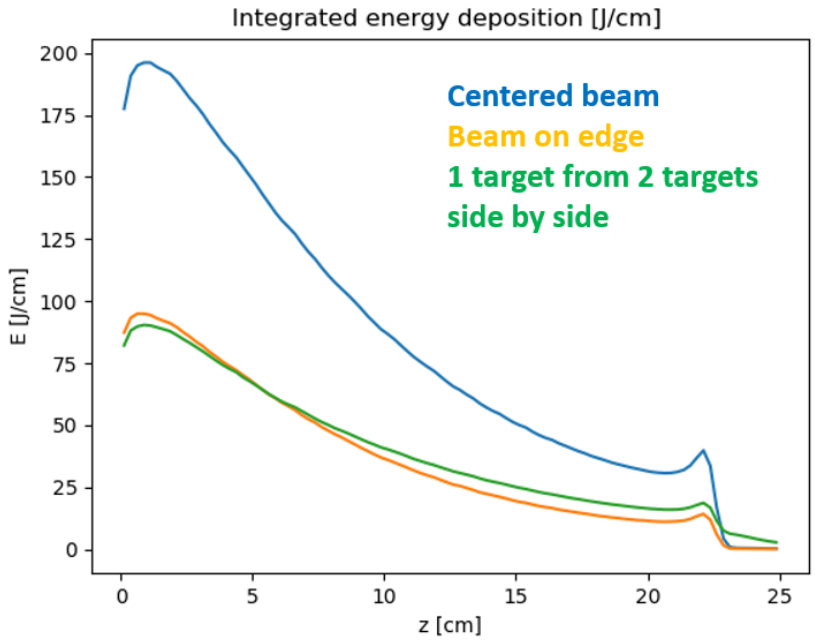

Figure 15. Comparison of energy deposition from all particles in the direction of the proton beam for three different configurations

4.1.2 Dependence of the Bragg peak on proton energy

The location and relative magnitude of the Bragg peak is highly dependent on the energy of the incoming protons. This is illustrated in figure 16, in which the deposited energy, integrated over the tungsten section perpendicular to the beam, is plotted along the beam direction for three proton energies: 500 MeV (green), 800 MeV (orange) and 1300 MeV (blue). With less energetic protons, the peak occurs closer to the front face of the target, is much higher, and has steeper gradients. For further illustration figure 17 shows the energy deposition in a cut through in the middle of the block with a 500 MeV beam. This situation needs to be avoided as it could lead to undesired large internal stresses. In the current design of the STS target (with

a proton energy of 1300 MeV), this is not a concern. With more energetic protons, most of the energy has already been lost before the protons come to rest. Therefore, the Bragg peak will be less pronounced, more spread out, and further along the target. This is visible in the 1300 MeV results (blue line) in figure 16, where only a small peak occurs around z = 43 cm. No peak is present in a 25 cm tungsten target with 1300 MeV as the particles travel all the way through a 25 cm thick target.

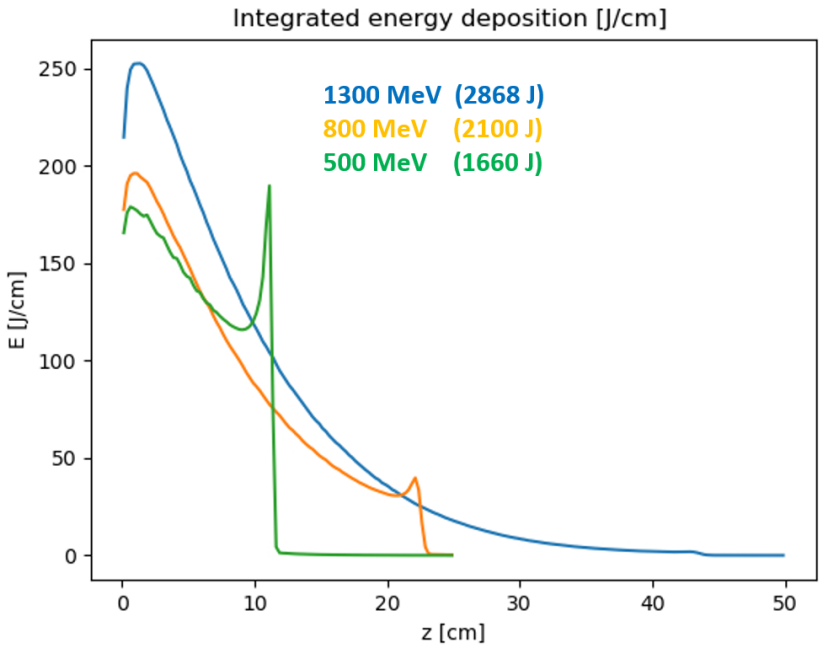

Figure 16. Illustration of the effect of the proton energy on the Bragg peak. The energy deposition (from all particle species) in a tungsten block in the direction of the proton beam is shown for 3 proton energies: 1300 MeV (blue), 800 MeV (orange), 500 MeV (green). The total energy deposited is listed for each case as well.

4.1.3 Energy deposition with STS-like conditions

In STS, the proton energy is expected to be 1300 MeV with a range from 1100 MeV to 1350 MeV. To replicate STS-conditions further, the tungsten block is followed by a stainless-steel block. In Figure 18 , the energy deposition along the beam direction is shown for proton energies of 1100, 1300 and 1350 MeV. The sudden decrease in energy deposition at the material boundary (z = 25 cm) is due to the differences between tungsten and stainless-steel. A very small Bragg peak is visible for 1100 MeV in the Stainless-Steel section around z = 43 cm, where the energy deposition suddenly drops to a negligible value. As the magnitude of the energy deposition are relatively small, this is not expected to be significant for stress analysis.

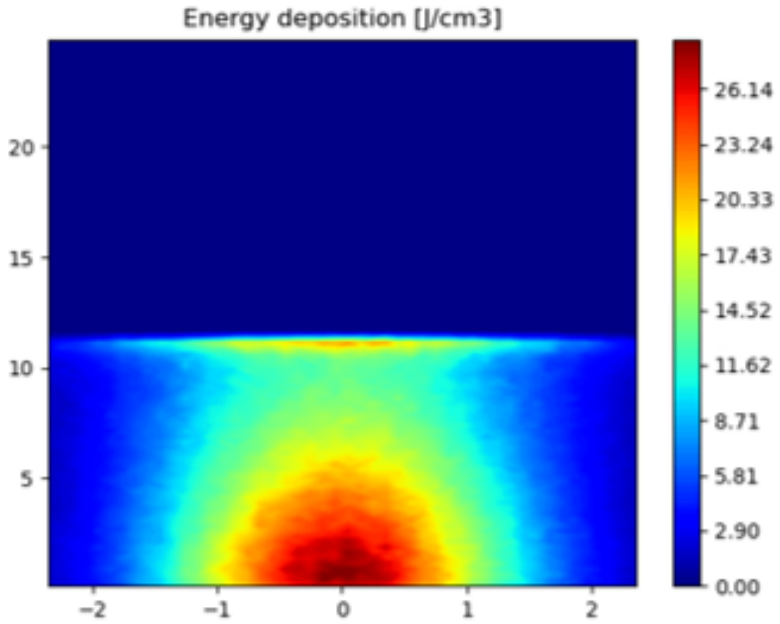

Figure 17. With a proton energy of 500 MeV, the Bragg peak (around z =11 cm) reaches almost the same local intensity as the initial peak close to the proton source. This figure shows the local energy deposition in the horizontal section through the vertical mid-plane (y=0 cm) of the tungsten block for a 500 MeV proton beam.

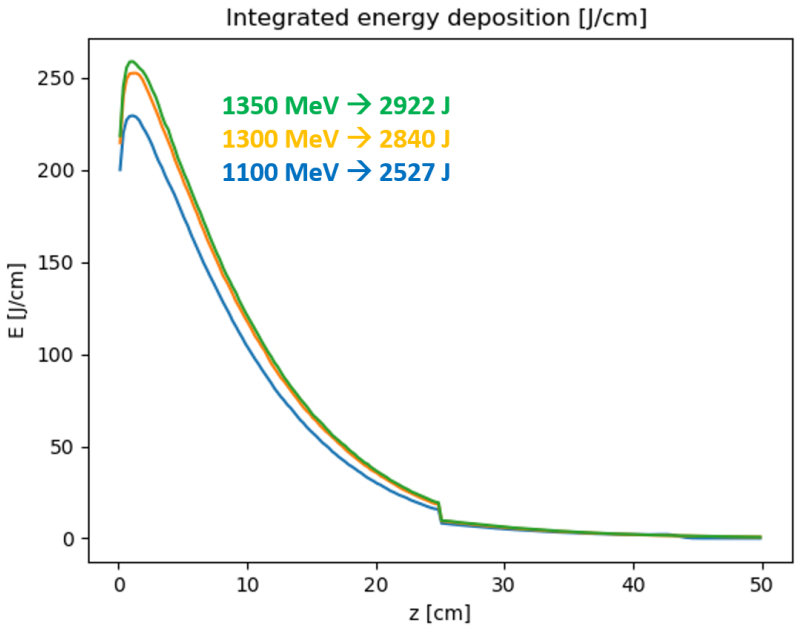

Figure 18. Energy deposition in a 25 cm tungsten block followed by a 25 cm Stainless Steel block for relevant STS proton energies. Also the total energy deposited (per pulse) in the blocks is listed.

4.1.4 Nominal vs squeezed beam

Next, we examine the influence of the beam shape on the total energy. For these simulations, the tungsten blocks have been shortened to 22 cm to avoid any undesired effects of the Bragg peak. For each of the 3 layouts, we examine impact with 1) a nominal beam profile, 2) a squeezed beam profile, and 3) a squeezed beam profile on a block with longer width (9 cm instead of 6 cm). The results are summarized in Table 6. A detailed energy distribution for some of these layouts can be found in the figures in appendix C.

A clear effect of the squeezed beam is a lower maximum local energy deposition. The squeezed beam profile has a 35% larger surface area ($\propto FWHM_x FWHM_y$) than the nominal beam. Therefore, the protons are more spread out which results in a less concentrated energy deposition. The differences in total energy deposition between the nominal and squeezed beam cases are mostly due to the number of protons hitting the target. With the squeezed beam, many protons are simply missing the target and cannot contribute. With a wider target (9 cm), this is no longer the case, and the total energy depositions are similar the those with a nominal beam.

Table 6. Summary of the energy deposition results with a target length of 22 cm.

Lay-out	Total energy deposited [J]	Maximum local energy deposition [J/cm3]	Number of protons incident on target	Percentage of protons hitting the target	Average energy deposition per incident proton [MeV]
Beam on center - nominal	2075	30	2.9428e13	98	440
Beam on edge l - nominal	908	27	1.4738e13	49	384
Two targets side by side - nominal	1930 → 965 per target	29	2.71677e13	91	443
Beam on center - squeezed	1699	22	2.45278e13	82	432
Beam on edge - squeezed	1002	21	1.48861e13	49	420
Two targets side by side - squeezed	2076 → 1049 per target	22	2.87386e13	96	455
Beam on center - squeezed – 9 cm	2076	22	2.86346e13	95	452
Beam on edge - squeezed – 9 cm	1022	21	1.5000e13	50	425
Two targets side by side - squeezed – 9 cm	2138 → 1069 per target	22	2.89369e13	96	461

4.1.5 Energy deposition in three-block configuration

Table 7 summarizes the results of the energy deposition analysis with the three-block configuration (section 3.1.2).The number in the case name refers to the position of the beam center. An ‘s’ is added to the name if a squeezed beam is used. For example, B1 refers to the case with a nominal beam centered on the first block, B23s refers to the case with a squeezed beam centered between block 2 and 3. The results are very similar to those of the simplified configuration. Files detailing the energy deposition as a function of

position have been made available to the STS analyst for thermal and stress analysis.

Table 7. Summary of the energy deposition in the three tungsten blocks and the tantalum cladding (on block 3) of the three-block configuration.

Case	Total [J]	tungsten block 1 [J]	tungsten block 2 [J]	tungsten block 3 [J]	tantalum cladding [J]	Maximum [J/cm3]
B1	2111	2067	40	2	0.2	30
B12	1937	964	996	6	0.5	29
B2	2163	40	2083	37	4	30
B23	1946	6	959	906	74	29 (W), 25 (Ta)
B3	2140	2	36	2063	39	30 (W), 23 (Ta)
B1s	1922	1710	208	3	0.2	22
B12s	2116	1046	1051	17	2	22
B2s	2162	209	1744	194	16	22 (W), 7 (Ta)
B23s	2125	18	1048	1014	45	22 (W), 19 (Ta)
B3s	1950	3	192	1710	44	22 (W), 17 (Ta)

Next, the energy deposition is calculated for the simplified three-block configuration (section 3.1.3) for a nominal beam impact with σ = 0.6 cm in the middle of the center block. The smaller beam leads to a much higher local energy deposition up to 85 J/cm3. The total energy deposition remains similar as before with 2251 J. A figure with more details on the energy distribution can be found in appendix C.A file detailing the energy deposition as a function of position has been made available to STS analyst for thermal and stress analysis.

Finally, the energy deposition is calculated for the simplified three-block configuration with cladding for a nominal beam impact with σ= 1 cm directed towards the center of the third, cladded block. The total and maximal energy deposition values in the tungsten and cladding are listed in table 8 for each case. Files with full details of the energy deposition as a function of position have been made available to STS analyst for thermal and stress analysis.

Table 8. Summary of the energy deposition in the simplified three-block configuration with cladding

Cladding	Total [J]	W 3 [J]	Cladding [J]	Max in W [J/cm3]	Max in cladding [J/cm3]
Tantalum	2151	2069	40	32	24
Niobium	2140	2073	25	32	14
No cladding	2115	2072	-	31	-

4.2 ACTIVATION

4.2.1 Source distribution

The tungsten block is divided into 45 cells (3x3x5) to approximate the effects of the non-uniform activation source. Figure 19 gives an overview of the distribution of the source within the 3x3x5 mesh. The block that receives the most protons in the front center radiates ≈13 % of the total source, followed by the two cells behind it in the direction of the beam, which contribute respectively ≈9% and ≈5%. Another ≈5% is radiated from the front cells on top and bottom relative to the front center cell. The front cells left and right from the center block contribute slightly less (≈4%), which is due to the different block size (2 cm and 1.6 cm per cell in respectively the x- and y-direction). Further away from the beam impact location, at the back of the block, there is only a very small source.

With longer decay time, the source becomes slightly more spread out with the center cells along the proton beam direction radiating relatively lower compared to the rest of the cells. Differences go up to 2% for the highest source. The main aspects of the distribution remain the same.

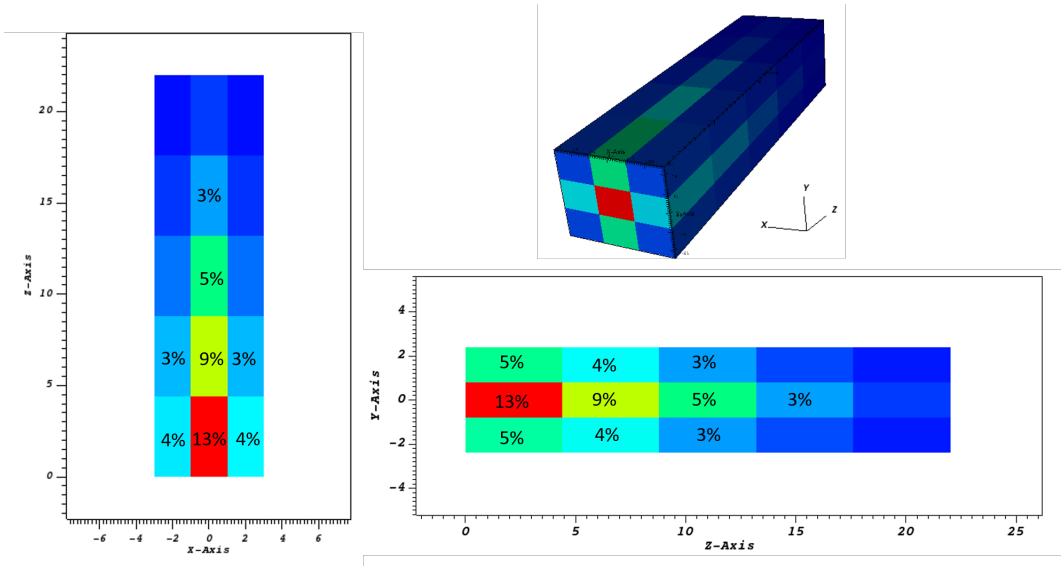

Figure 19. Illustration of the source distribution (approximate values). The rounded edges of the tungsten block geometry are not shown in this figure, which only serves to give more details on the source distribution.

4.2.2 Activation dose around one tungsten block

In figure 20 and 21, we show the dose rate 1 min after irradiation for respectively a horizontal and vertical cut through the geometry in the vicinity of the tungsten block surrounded by air (no steel shielding present). We also show the direction of the proton beam and the approximate detector locations at 30 cm from the tungsten block. Comparing the zone in front and at the back of the target ($z < 0$ cm and $z > 22$ cm), there is a clear asymmetry because of the distributed source. As the largest source comes from the front center of the tungsten block, the highest dose rates are found close to this area. Looking at a constant

distance from the target, the lowest dose rates are at the back. The dose rate profiles from left to right and from top to bottom are approximately symmetric.

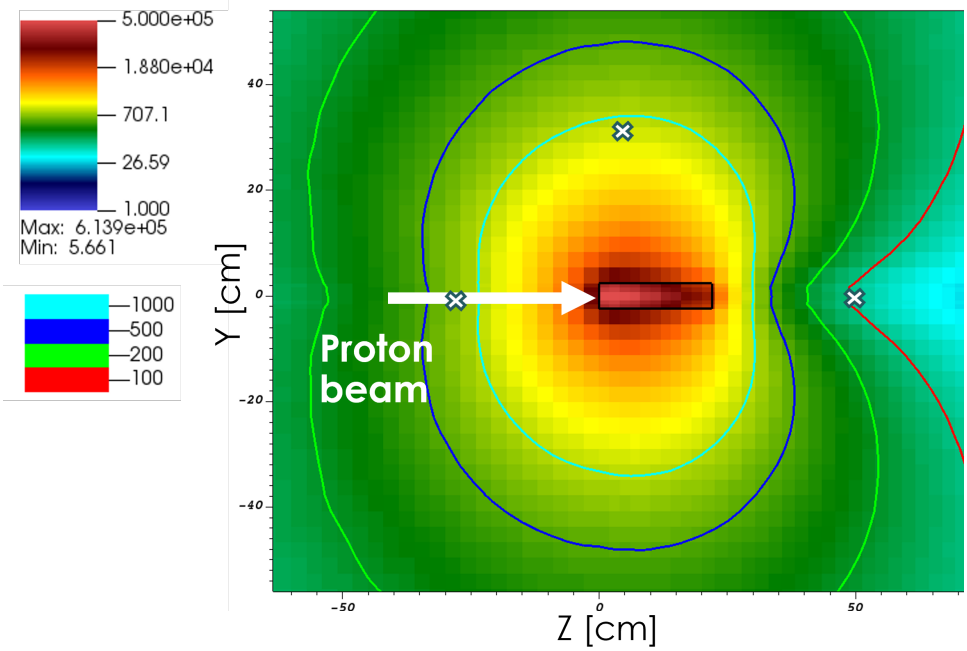

Figure 20. Dose rate 1 min after irradiation in the x=0 plane (vertical cut). Approximate detector locations are marked with crosses

The detector that receives the highest dose is located above the target, followed by the one at the side of the target. This difference can be explained by the smaller length of the tungsten block in the vertical direction (4.8 cm) compared to the horizontal direction (6 cm), which results in less self-shielding. As expected, the difference in dose between the front and the back detector is very large and reaches an order of magnitude.

The dose rates at the 4 detectors are shown as a function of the decay time in figure 22. One minute after proton beam shutdown, the dose rate at 30 cm from the tungsten block reaches approximately 1000 mrem/h at the top of the block. After 1 day, this decreases to 100 mrem/h, and to only 10 mrem/h after 7 days. Table 9 gives more details on the dose rates at the detector locations.

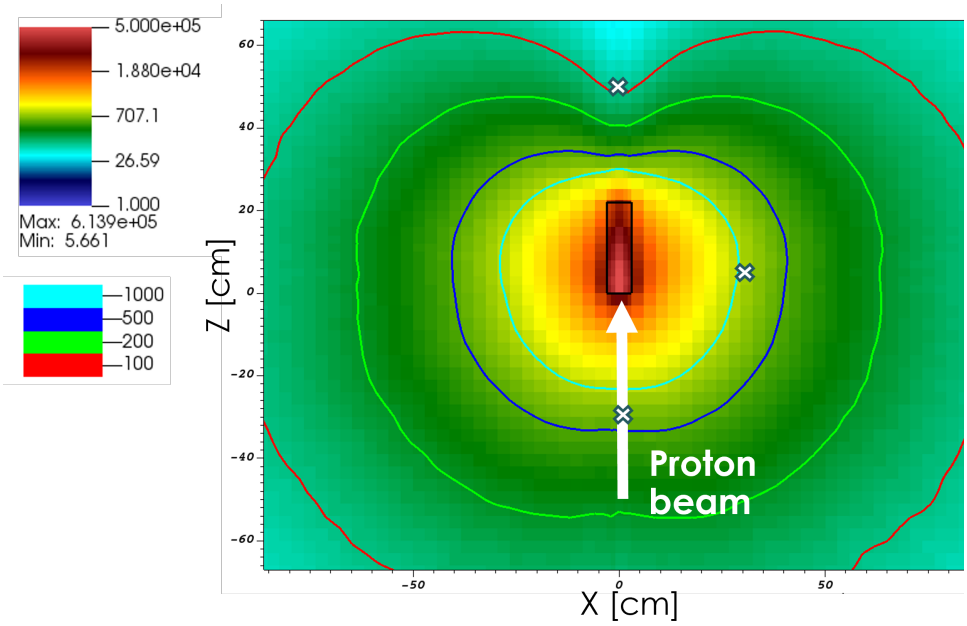

Figure 21. Dose rate 1 min after irradiation in the y=0 plane (horizontal cut). Approximate detector locations are marked with crosses.

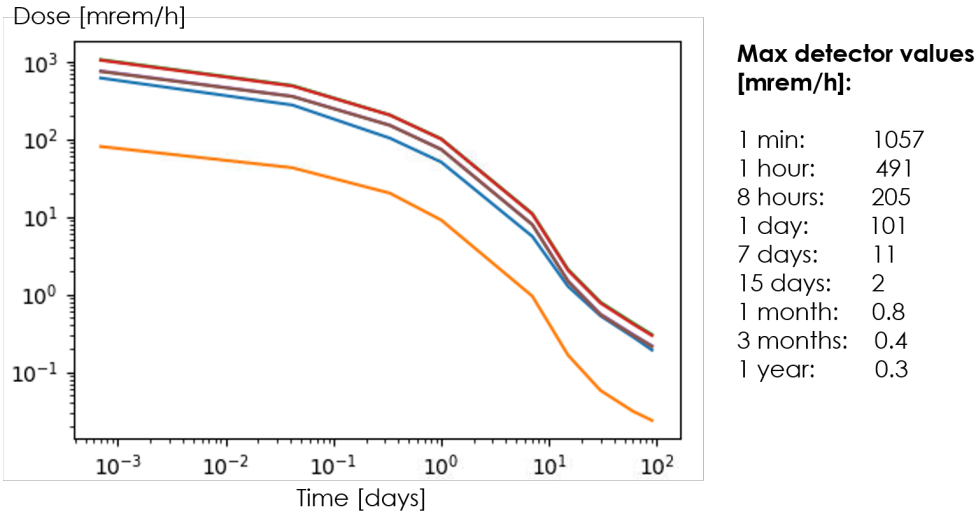

Figure 22. Dose rates vs decay time for the detectors at 30 cm from the tungsten block

4.2.3 Comparison between a distributed and a uniform source

As the tungsten block sees the same total amount of protons, there is no difference in the total source strength between the distributed source on the 3x3x5-mesh and the source that is uniformly distributed over the whole tungsten block. Therefore, the differences in dose rate are entirely due to the different distribution of gamma activation source and the resulting differences from self-shielding.

Comparing the dose rates in figure 23, we can clearly see the effect of the different source distribution.

Table 9. Detector values [mrem/h] for the dose rate at 30 cm from the tungsten block as a function of decay time after irradiation

Decay time	Front [mrem/h]	Back [mrem/h]	Top [mrem/h]	Side [mrem/h]
1 min	613	80	1057	755
1 hour	275	43	491	357
8 hour	103	20	205	152
1 day	51	9	101	74
7 days	6	1	11	8
15 days	1	0.2	2	2
1 month	0.5	0.06	0.8	0.6
3 months	0.3	0.03	0.4	0.3
1 year	0.2	0.02	0.3	0.2

With the distributed source, there is no symmetry between the back and front, which is present for the uniform source. The largest differences are thus seen for the detector in front and at the back of the tungsten block. With a uniform source, the detector in front of the block sees only half of the dose, while the detector in the back is receiving a 3-4 times higher dose, with respect tot the case with the distributed source. The detector above the tungsten block and on the side are respectively ≈10% and ≈30% higher for the uniform source compared to the distributed source.

In figure 24, we show the ratio $R = D_1/D_{3x3x5}$ between the dose resulting from the uniform source (D_1) and that from the distributed source (D_{3x3x5}). The red colors indicate a small ratio, for which the distributed source gives a higher dose than the uniform source. The blue colors indicate a high ratio in the regions where the uniform source gives higher dose rates. The blue line indicates a ratio of 1, for which the dose rates are the same for both sources. Higher dose rates for D_{3x3x5} are observed in a cone in front of the tungsten block, where the source is higher with the distributed source. Outside of this cone, the dose is lower for the distributed source. The dark blue zone marked by the yellow line indicates the region where the dose is more than twice as low as with the uniform source.

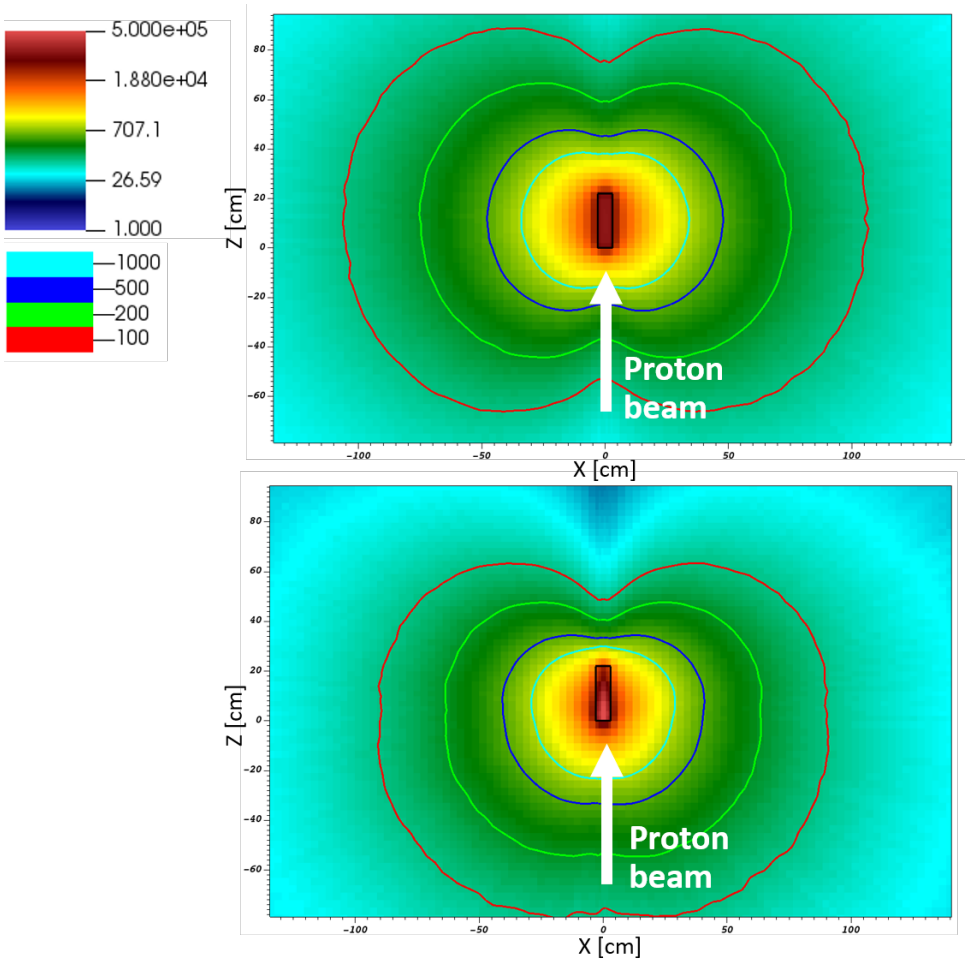

Figure 23. Dose rate [mrem/h] around the tungsten block 1 min after irradiation for the uniform and the distributed source (respectively the upper and lower figure)

4.2.4 Dose rate after one pulse

The dose rates at the detector after just one pulse are listed in table 10. One minute after one pulse, the dose rate on top of the block (maximum value at the detectors) is 500 mrem/h. It decreases quickly with values to 136 mrem/h after 15 mins and 36 mrem/h after one hour. Looking at figure 25, we can compare the source strengths as a function of decay time for an irradiation history of 1 pulse, 5 pulses, and the full pulse history. Clearly, after only 1 or 5 pulses the source strength decreases much more quickly than after the full irradiation history as less long-living radioactive isotopes have been built up. It is noteworthy to point out that 5 full intensity pulses give a higher dose rate 1 min after irradiation than the full irradiation history. This is because the final pulse series in the irradiation pulse plan is at only 25% of the full intensity.

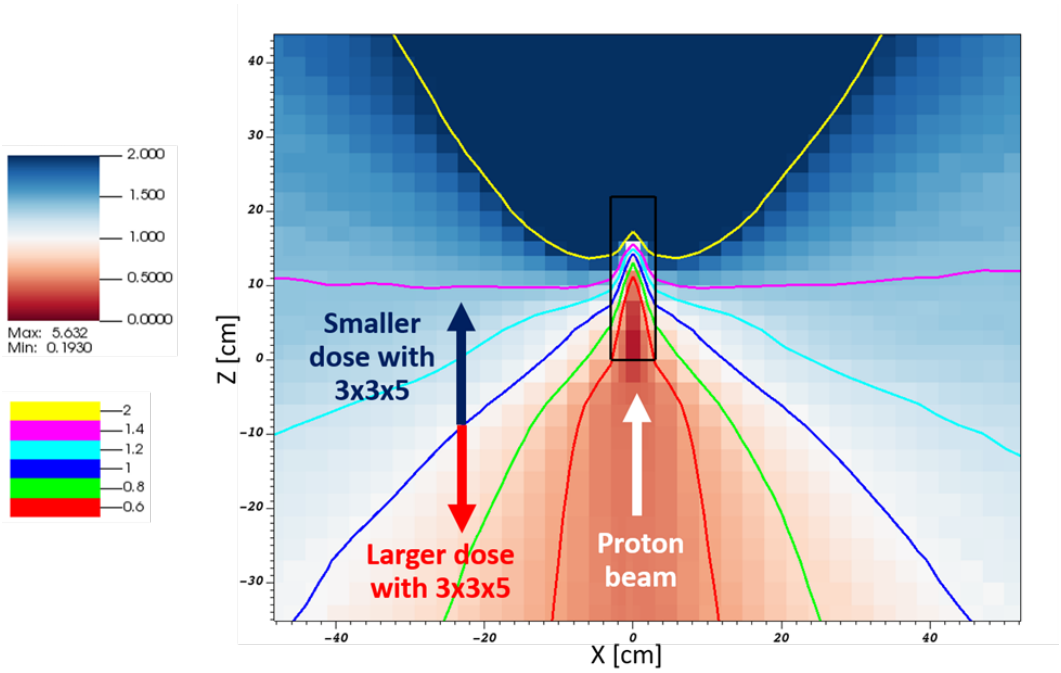

Figure 24. Ratio of the dose rates resulting from the uniform source to that with the distributed source (respectively the upper and lower figure).

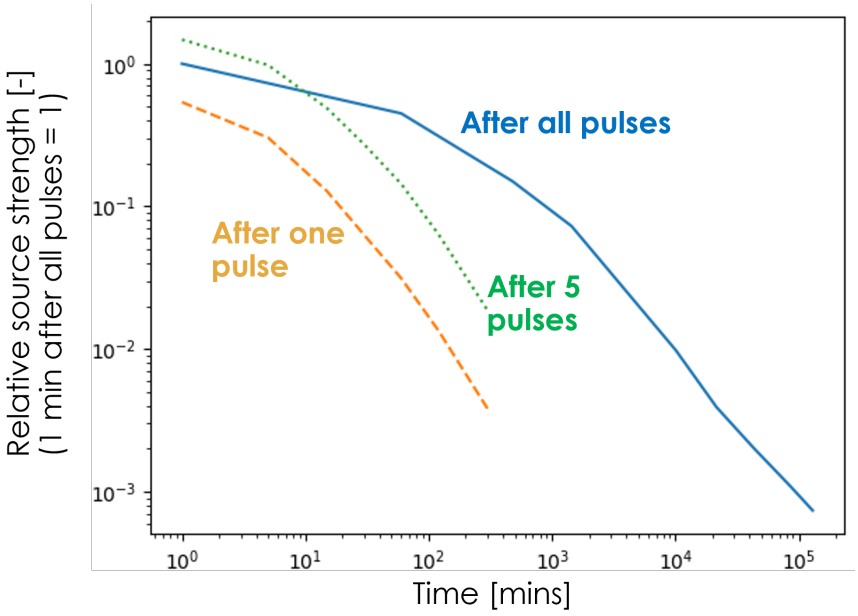

Figure 25. Source strength versus decay time after irradiation with one pulse, 5 pulses, and all pulses, relative to the source strength 1 min after irradiation with all pulses.

Table 10. Detector values [mrem/h] after one pulse. The relative statistical errors are <1%.

Decay time	Front [mrem/h]	Back [mrem/h]	Top [mrem/h]	Side [mrem/h]
1 min	353	25	500	347
5 min	184	17	285	200
15 min	81	9	136	96
30 min	42	5	74	53
1 hour	20	3	36	26
2 hours	8	1	13	10
5 hours	2	0.3	4	3

4.2.5 Effect of averaging in pulse history

When separate pulses are modeled instead of considering continuous irradiation, large differences in source strength can be expected immediately after a pulse. At longer decay times, the difference decreases. As the total amount of irradiation is the same, the same amount of radioactive atoms is created. The distribution in time, however, is different. The source (and dose) from short-lived gamma-emitters is present immediately after the irradiation but disappears shortly after. With a continuous irradiation history, these short-lived isotopes are spread and decayed out over the full time interval. For long-lived isotopes, for which the decay time is long compared to the time differences in irradiation history, there is no significant difference. This is demonstrated in figure 26 , in which the activation source strength is compared for a continuous and pulsed history for the first sequence of 5x5 proton pulses in a time interval of 100 mins. The left graph graphically represents the two histories with pulses of 0.001s (blue) and continuous irradiation (orange). In the right graph, source strengths are compared a function of decay time. The dashed orange line represents the results from the continuous irradiation history. The source strength from the pulsed sequence (the dotted green line) is ≈30% higher than with a continuous history after 1 minute of decay. The difference decreases with decay time: after 1 hour, only 5% difference remains. When we start counting the decay time after the full 100 min interval (blue line) instead of immediately after the last pulse, source strengths from the pulsed sequence are lower than those from continuous irradiation over the same time interval. At relevant decay times (2 mins and longer), the pulse length does not influence the result if it is sufficiently short. No meaningful differences have been observed between a pulse length of 0.1s and 0.001s.

We conclude that the source strength and thus also the dose rates are underestimated immediately after the last pulse when a continuous irradiation is assumed instead of a pulse sequence. The difference becomes smaller at longer decay times.

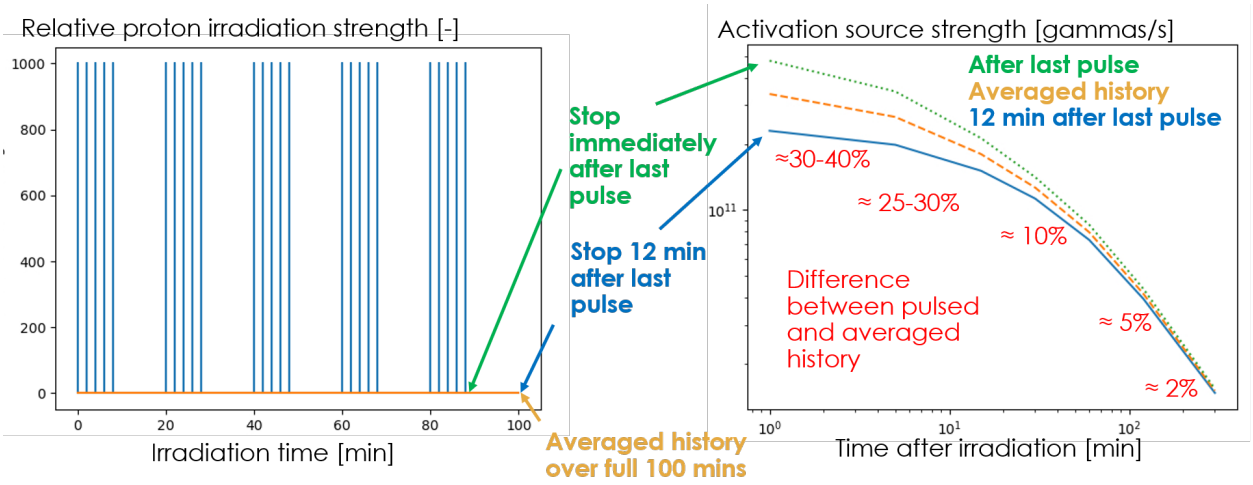

Figure 26. Source strengths resulting from a continuous irradiation history compared to those with a pulsed history.

4.2.6 High-fidelity analysis with 3-block configuration and detailed pulse plan

The high-fidelity analysis considers a configuration with 3 tungsten blocks and models each pulse separately. Steel shielding is not considered for this analysis. Dose rate maps for 1 min and 1 hour after irradiation are shown in figure 27. A clear asymmetry is present between the left and the right side, especially 1 min after the last pulse. This is due to the asymmetry in the pulse plan, in which the last pulse sequence is directed towards the center of the left tungsten block. The values at the left and right detector locations differ significantly for short decay times and converge towards each other for longer decay times (see figure 28 and table 11). As the pulse locations for the full irradiation sequence are symmetric across the centerline of the tungsten blocks, the difference is only due to the different distribution of the pulses in time.

Table 11. Dose rates [mrem/h] at detectors 30 cm from the tungsten blocks with the high-fidelity simulation (statistical uncertainty ≈1%)

Decay time	Right [mrem/h]	Left [mrem/h]	Top [mrem/h]	Front [mrem/h]	Back [mrem/h]
1 min	111	575	1350	883	100
5 min	111	419	1110	681	89
15 min	101	273	862	528	73
30 min	98	189	692	427	61
1 hour	82	123	532	331	47
2 hours	67	104	391	244	38
5 hours	50	50	276	122	28
1 day	19	19	106	48	10
7 days	2	2	11	5	1
15 days	0.4	0.4	2	1	0.2
1 month	0.2	0.2	0.8	0.5	0.07

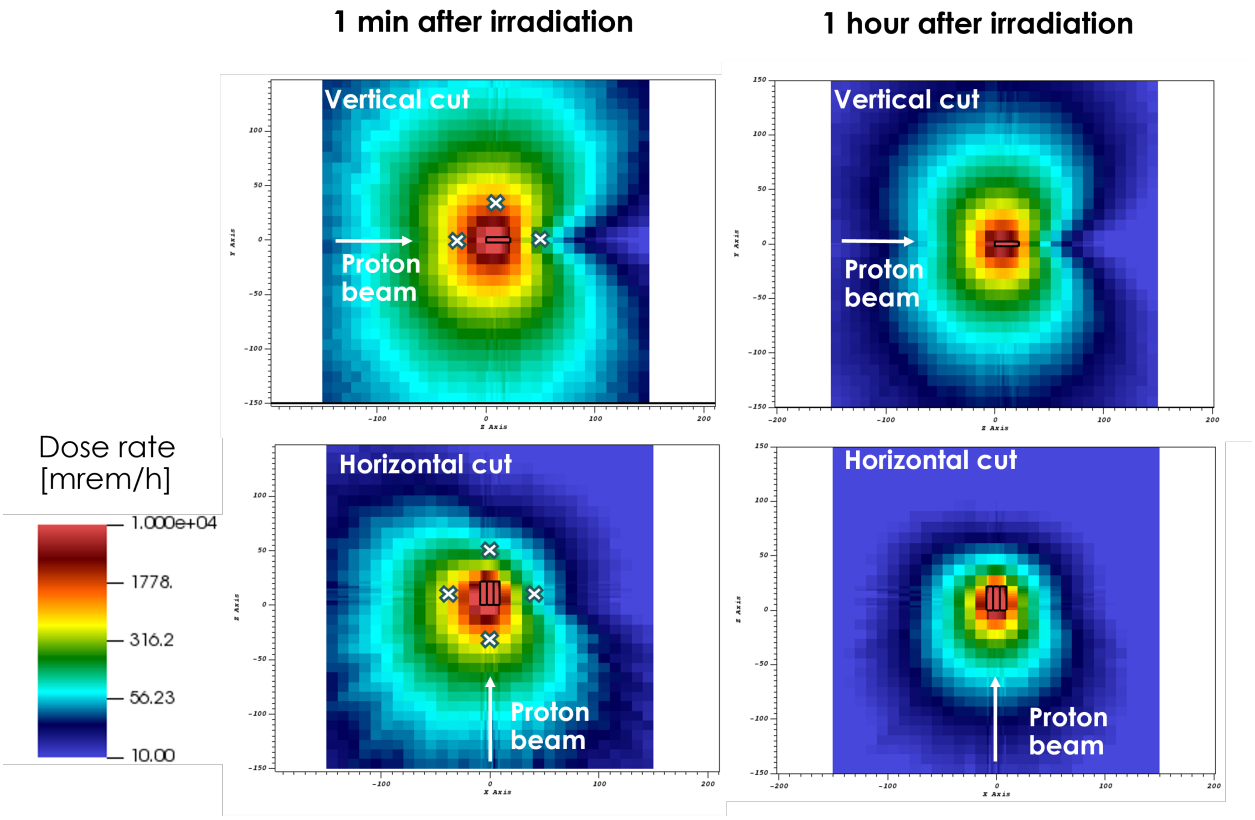

Figure 27. Dose rate maps after 1 min (left) and 1 hour (right) of decay time with the high-fidelity model. Approximate detector location at 30 cm from the tungsten are indicated with crosses.

Compared to the simplified analysis, the dose rates are very similar except for the detectors on the sides (see figure 29). This is expected as the tungsten blocks on the side, which are not present in the simplified model, provide a significant amount of self-shielding. For the other detectors (front, top, back), a very good agreement is observed, especially for longer decay times (> 1 hour). For small decay times (< 1 hour), slightly higher dose rates are present due to the detailed pulse history.

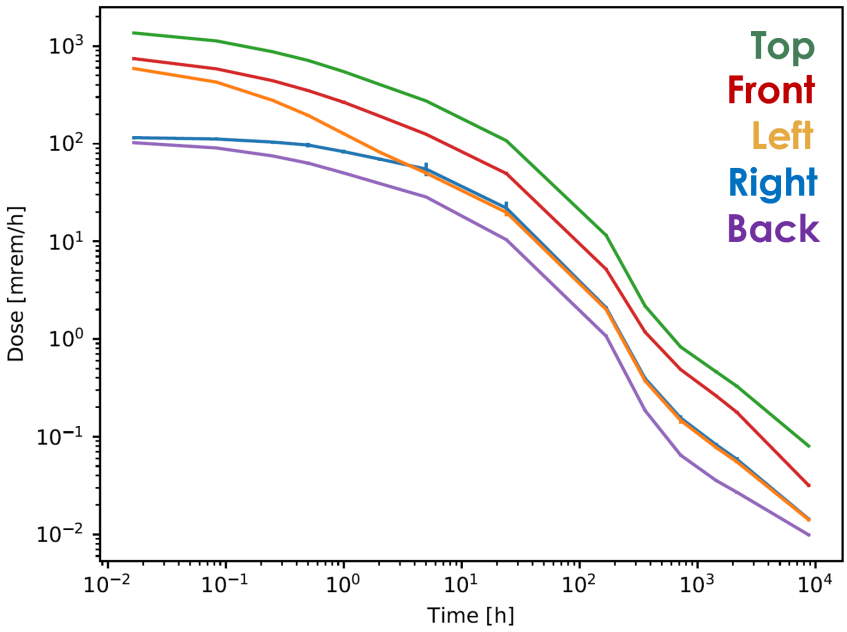

Figure 28. Dose rates [mrem/h] as a function of decay time [h] for the detectors 30 cm from the tungsten blocks from the high-fidelity simulation

4.2.7 Dose rates from activated tungsten with lead or carbon steel shielding

Shielding around the activated tungsten block is necessary to be able to clear the blue room as fast and as safe as possible after the experiment. By adding 2-inch lead shielding on all sides (see figure 30), the dose rates are reduced approximately 15 times. The resulting dose rates at the detector locations 1 hour after irradiation are shown table 12. To reduce the dose to ≈5 mrem/h 1 hour after irradiation, ≈8.5 cm of lead shielding is required. The activation sources from the simplified model have been used for this calculation.

Table 12. Dose rates at detectors with 2-inch lead shielding (not activated) around the activated tungsten 1 hour after irradiation. (Sources are taken from the simplified model)

	Dose after 1 hour [mrem/h]	Relative error [%]
Front	19	1.7
Back	4	1.7
Top	32	3.0
Side	24	2.0

It was decided to choose carbon steel as shielding material (because of easy and fast availability). With a 2-inch thickness, dose rates after 1 hour remain rather high with values >100 mrem/h at the top detector (see table 13). With a 4-inch thickness, all detectors remain below 30 mrem/h. For this calculation, the source terms from the high-fidelity model have been used.

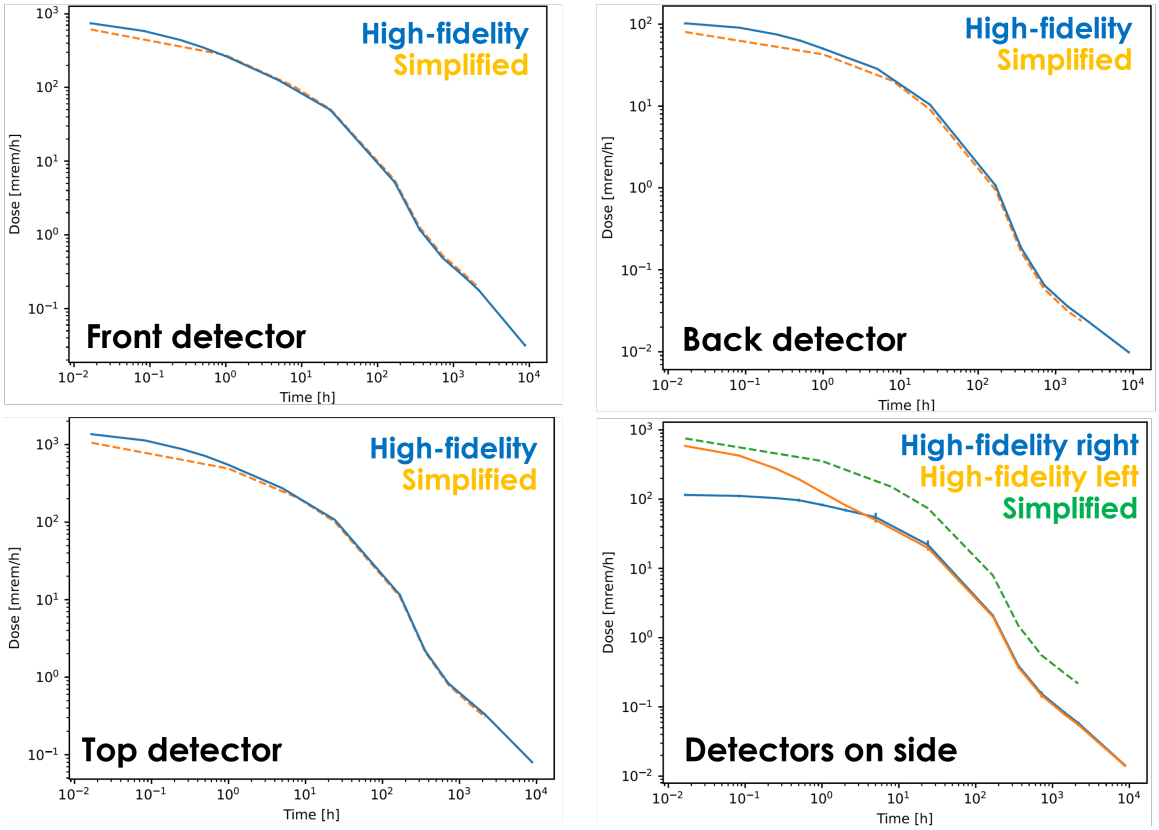

Figure 29. Dose rates [mrem/h] as function of decay time [h] for the simplified and the high-fidelity simulation.

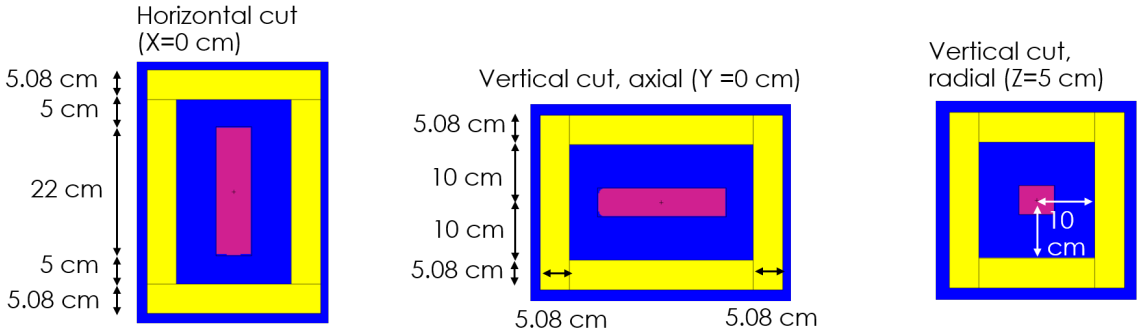

Figure 30. 2-inch lead shielding (yellow) around tungsten block (pink).

4.2.8 Activation of the carbon steel shielding

The steel shielding surrounding the tungsten blocks will become activated by the neutrons and protons emanating from the tungsten blocks during the experiment. The source strength in each activation cell is shown in figure 31 (left). As expected, the highest contribution comes from the inner shell surrounding all sides of the tungsten blocks (indicated with number 10), which is the most exposed to neutrons. Going outward (number 11 to 14), the source strength decreases. The steel at the back side (number 20 to 24) is

Table 13. Dose rates at detectors after 1 hour with carbon steel shielding. Statistical errors are <0.5%. (Sources are taken from the high-fidelity model)

	Dose after 1 hour [mrem/h] with 2-inch thickness	Dose after 1 hour [mrem/h] with 4-inch thickness
Right	25.3	5.5
Left	36.7	7.92
Top	128.6	26.8
Front	68.0	14.5
Back	15.5	3.35

exposed to less neutrons and more protons. This results in an overall lower source strength and a noticeably different shape of the source strength as a function of time due to the different activation products. The dose rates at detector points 30 cm from the steel surface are shown in the right graph of figure 31. For small decay times (1 hour or less), high values around 50-100 mrem/h are observed. After 1 day, the dose rates decreased more than an order of magnitude. These dose rates are due to the total dose of the activated steel only. To obtain the total dose, the contribution of the activated tungsten inside the steel shielding needs to be added.

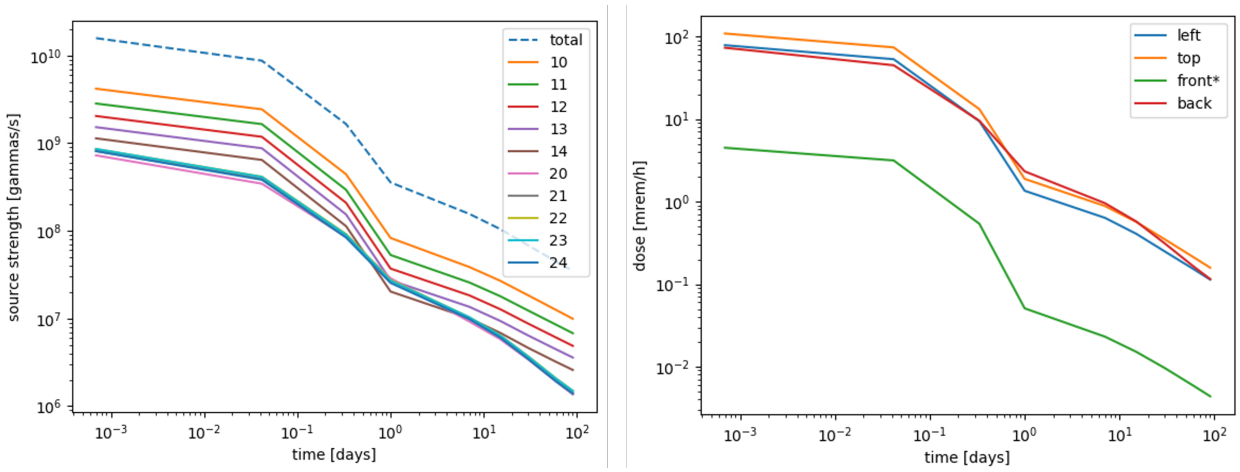

Figure 31. Activation source strength in each activation cell of the steel shielding as a function of time (left) and the resulting dose rates at the detector point 30 cm from the steel shielding (right)

The total dose rate 1 hour after irradiation (see table 14) is highly dominated by the contribution of the steel and causes concern because it is reaching estimated values closely approaching 100 mrem/h, which is the limit to be considered a high radiation area. The main gamma emitter in the activated steel is Mn-56, which emits strong 0.85 MeV and 1.8 MeV photons (see figure 32 bottom). Mn-56 is produced by the (n,p) reaction of a highly energetic neutron (> 1 MeV) in Fe-56 (see figure 32 top), one of the main nuclei that is present in steel. As Mn-56 has a half-life of 2.5 hours, the estimated dose rate considerably decreases after 8 hours, reaching only 21 mrem/h in total. Waiting 8 hours after irradiation before entering the room is, therefore, an excellent mitigation strategy to reduce exposure. Another option to reduce dose rates is to add additional shielding. A 0.5-inch lead blanket, that is added after irradiation, reduces the total dose after 1

hour by approximately 35-40 %. The dose that a person will receive to go in and lay a blanket over the experiment has not been evaluated.

Table 14. Dose rates [mrem/h] from activated steel and activated tungsten at 30 cm from the steel shielding. The listed values from tungsten are the dose rates coming through the steel shielding.

	Left	**Top**	**Back**
After 1 hour:			
Total	**57**	**87**	**46**
From steel	53	74	31
From tungsten	4	14	1.7
After 1 hour with unirradiated lead blanket:			
Total	36	55	28
From steel	34	46	27
From tungsten	2.6	8.9	1.1
After 8 hours:			
Total	**11**	**21**	**11**
From steel	9.4	13	9.5
From tungsten	1.7	7.5	1.0

The effect of impurities in the steel on the dose after 1 hour is minor. We compare dose rates from 3 types of steel: Carbon steel (used for the analysis before), Steel 1020 with a low level of impurities, and steel A387 for which we chose a high level of impurity. The resulting dose rate values after 1 hour are listed in table 15. Comparing carbon steel with high-impurity steel A38, only a small difference is observed. The difference of carbon steel with low-impurity steel 1020 is much bigger. The main gamma emitter remains Mn56, which is produced by Fe56, one of the main isotopes in steel. The percentage of iron in steel 1020 is lower than in carbon steel, resulting in lower dose rates.

Table 15. Dose rates [mrem/h] from activated steel for several material compositions of steel, 1 hour after irradiation

	Left	**Top**	**Back**
Carbon Steel	53	74	45
Steel 1020 (low impurity level)	38	53	34
Steel A38 (high impurity level)	54	75	44

A lead wall can provide another way to limit radiation dose for people that need to be in closer proximity to the activated fixture. We examine two geometries: 1) with the activated steel shielding present around the tungsten blocks, and 2) with bare tungsten without any shielding around it. We remind the reader that backshine from the room or components in the room has not been evaluated.

With the shielding present, the dominant contribution of the total dose rate comes from the activated steel. For this calculation, only this dose rate is considered, resulting in a slight underestimation of the total dose (<10%). Just before the lead wall, which is placed 30 cm from the steel shielding, dose rates up to 50 mrem/h are observed (see figure 33). The lead wall provides excellent shielding resulting in a maximal dose rate of 2 mrem/h behind the wall. Next the lead wall, dose rates up to 15 mrem/h are present.

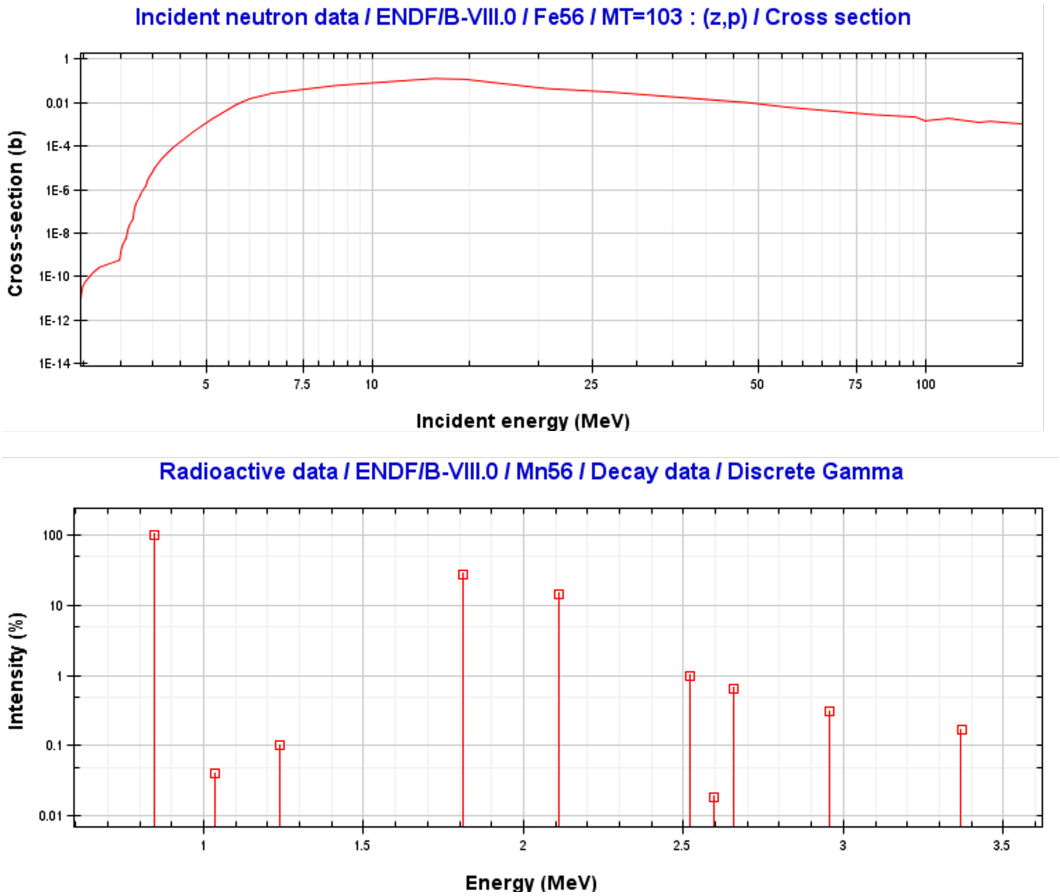

Figure 32. Incident neutron cross-section of Fe-56 (top) and the gamma emission spectrum of Mn-56 (bottom).Ref JANIS

Without shielding present, the activated tungsten causes dose rates up 95 mrem/h in front of the lead wall 1 hour after irradiation (see figure 34, left). Behind the lead wall, this is reduced to <10 mrem/h. Next to the lead wall, however, dose rates remain high reaching values up to 57 mrem/h (see figure 34, right).

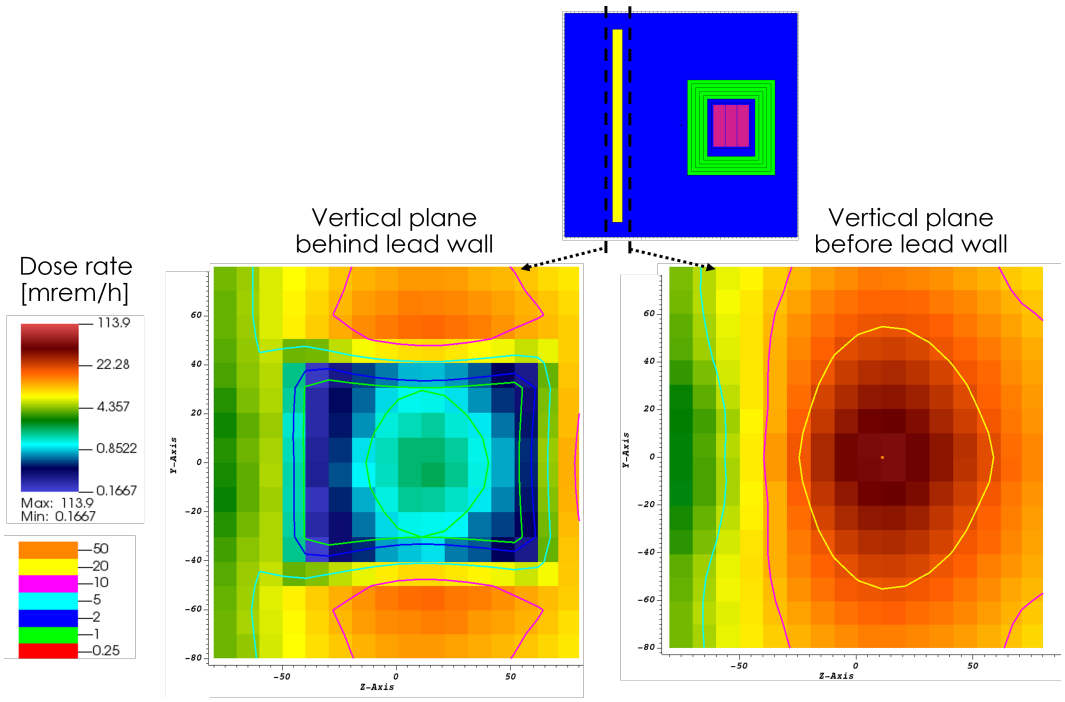

Figure 33. Dose rates 1 hour after irradiation from activated steel in a vertical plane just in behind (left) and just before (right) the lead wall.

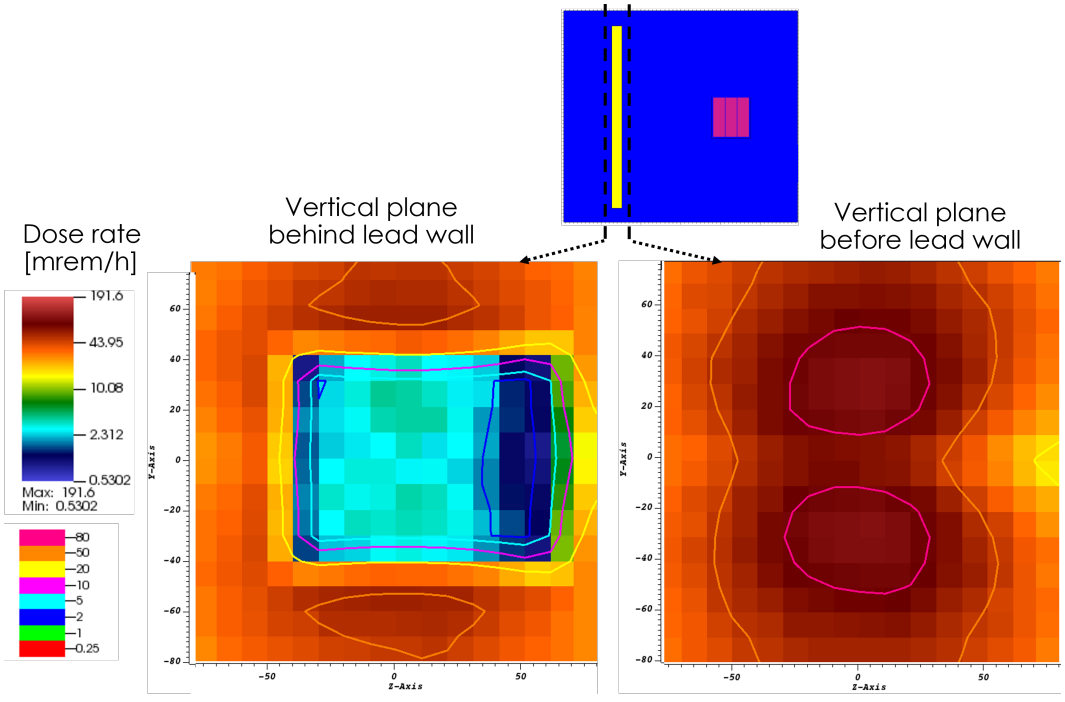

Figure 34. :Dose rates 1 hour after irradiation from activated tungsten, without steel shielding present, in a vertical plane just behind (left) and just before (right) the lead wall

4.2.9 Alternative shielding materials

If another material is used for shielding instead of carbon steel, activation dose rates can be very different. In this section, we examine aluminum Al6061 and lead as possible alternatives.

Aluminum is not considered a good shielding material as it has a very low density compared to typical shielding materials as lead and steel. It is examined here because of the easy short-term availability of aluminum blocks. With a 4-inch aluminum shielding around the activated tungsten, the dose rate from the aluminum shielding (not activated) reaches 110 mrem/h at the top detector (30 cm from the aluminum shield) 1 hour after irradiation. This is almost 8 times higher than with the 4-inch steel shielding. This dose rate alone is higher than the total dose rate with steel, including the contribution of activation products in the steel.

Table 16. Dose rates [mrem/h] 1 hour after irradiation with aluminum shielding

	Left	**Top**	**Back**
Dose from activated tungsten	34	110	15
Dose from activated Al6061	190	250	150
Dose from Al6061 with a high level of impurities	260	340	200
Total = Al6061 + tungsten	220	360	170
Total with a high level of impurities = Al6061 (high-impurity)+ tungsten	294	450	215

Aluminum gets highly activated in the presence of 6-20 MeV neutrons. Na-24, which has two very intense decay gammas of approximately 1.3 and 2.7 MeV is produced by (n, α) reaction in one of the main isotopes of aluminum, Al-27 (see figure 35). The dose rates resulting from the activated aluminum are shown as a function of time with the dashed lines in figure 36 (left). The full lines show the values for steel shielding for comparison. For short decay times (<1 week), dose rates are substantially higher for aluminum than for steel. The sudden drop in dose rate is related to the disappearance of Na-24, which has a half-life of 15h. The dose rates for 1 hour of decay time are also listed in table 16. Adding the dose rates from aluminum and tungsten brings the total to 360 mrem/h at the top detector. When a conservative level of impurities is added in aluminum, the dose rate increases to 450 mrem/h. This is almost as high as the dose rate from bare tungsten, without any shielding present. We conclude that replacing steel with aluminum is not a reasonable option.

With lead as shielding material, spallation reactions result in a variety of isotopes contributing to the dose. At most decay times, the dose rates are lower with a 4-inch lead shielding compared to a 4-inch carbon steel shielding (see right graph in figure 36, in which the dashed and full lines represent dose rates from respectively lead and steel). At 1 hour of decay time, lead shielding results in 4-5 times smaller dose rates than carbon steel. In appendix 6, we explore a few shielding options that combine lead and steel.

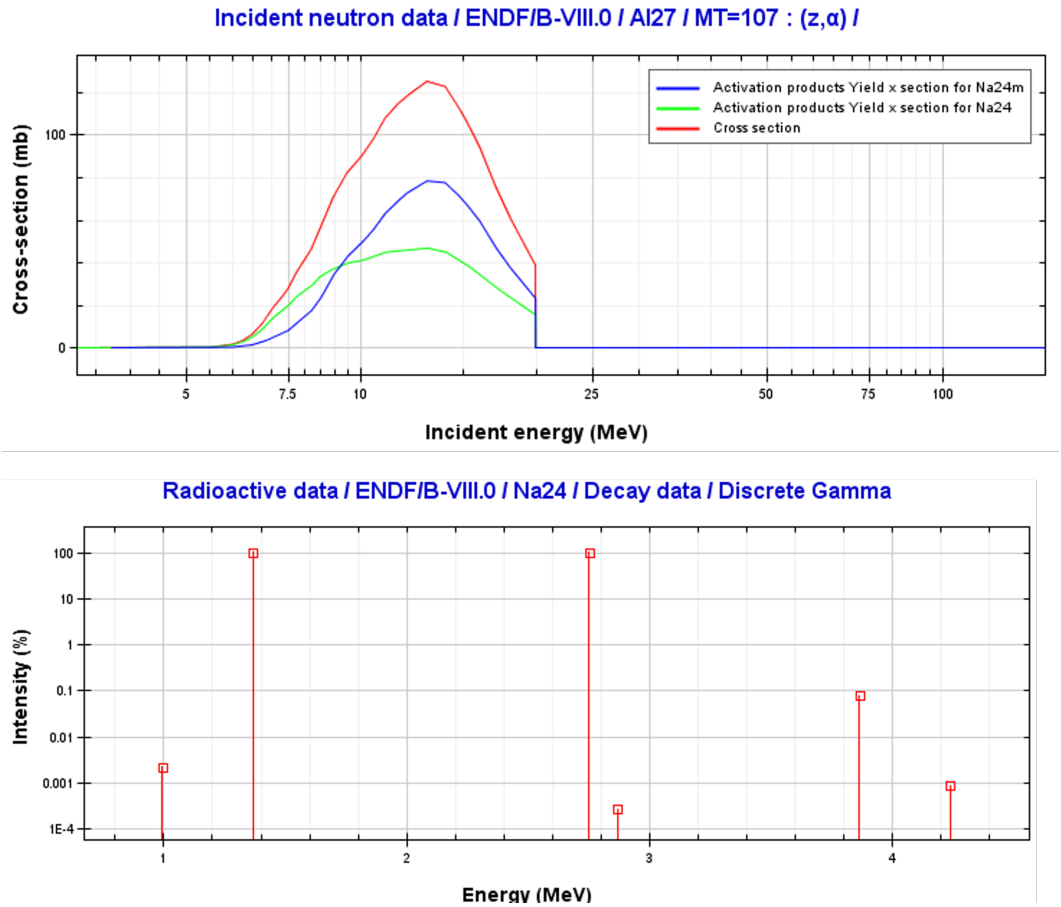

Figure 35. Incident neutron cross-section, and Na-24 and Na-24m activation yield cross-sections of Al-27 (top) and the gamma emission spectrum of Na-24 (bottom).Ref JANIS

4.2.10 Activation of the cladding material

For small decay times (< 1 week) dose rates at 30 cm from the tungsten blocks, the tantalum cladding does not increase the order of magnitude of the dose rates. For longer decay times, there is a clear increase, but this should not cause concern as the total dose rate is rather small (< 15 mrem/h). This is illustrated in figure 37, in which we show the dose rates as a function of time for detectors at 30 cm from the tungsten blocks. The dose rates are similar in magnitude to those obtained with the high-fidelity model. As the cladding is only present on the right tungsten block, the effect of the activated cladding will be most visible at the right detector, while the left detector point is shielded from the tantalum by the other two tungsten blocks. By comparing the left and right detector values in figure 37, we start seeing a clear difference after 1 week. Dose rates at all detectors, however, remain small.

The activation source strengths from the niobium cladding are more than 2 times smaller than with tantalum cladding. Dose rates with niobium cladding are, therefore, expected to be smaller than for tantalum cladding.

We remind the reader that this analysis is highly simplified and only gives an indication of the order of magnitude. The presence of cladding will increase the dose rates, especially in the front/top section of the

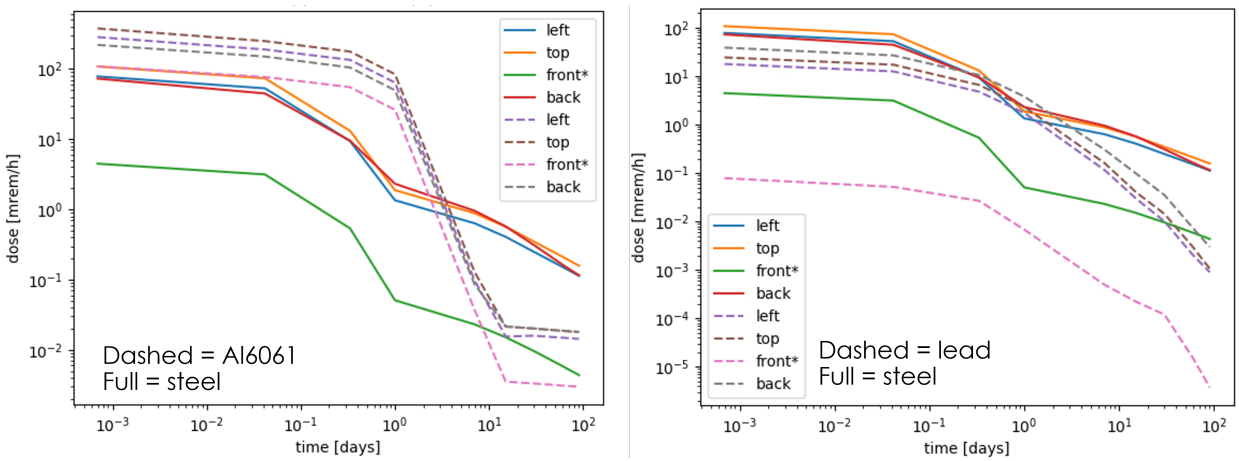

Figure 36. Dose rates vs time for steel and Al6061shielding (left), and steel and lead shielding (right), originating from the activated shielding material (dose rates from activated tungsten not included), at detector points 30 cm from the shielding

configuration. As this analysis does not consider a distributed activation source, this effect is not evaluated here. If a higher accuracy is required, a more refined analysis needs to be done.

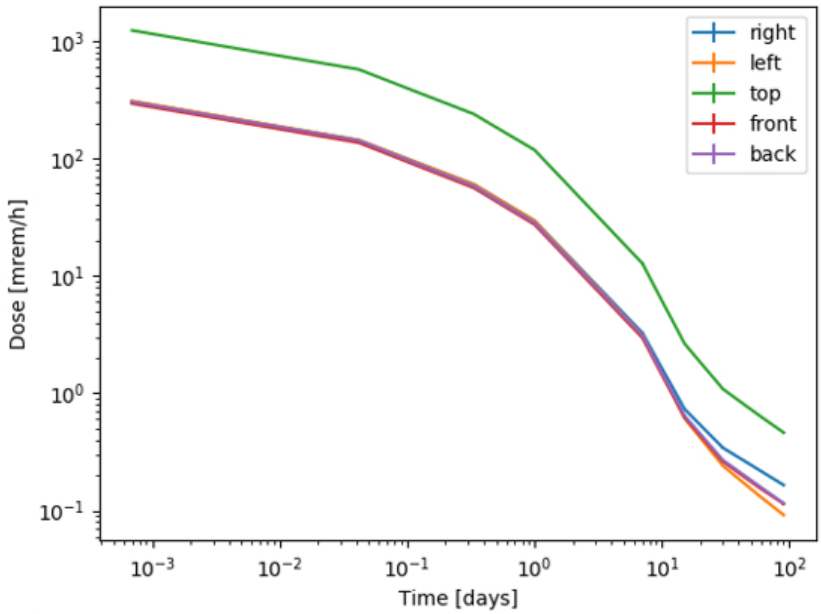

Figure 37. Dose rates [mrem/h] as a function of time after decay for detectors at 30 cm from the tungsten blocks with tantalum-cladding on the right block (statistical errors < 5%)

4.3 WINDOW IRRADIATION

To examine the performance of potential window materials in a radiation environment, the protons and neutrons emanating from the tungsten blocks can be used to expose materials for the second TVP mirror. While the irradiative conditions are not identical to those at the second TVP mirror (located near the top of the TVP), the resulting irradiation damage can give a first evaluation and indicate whether more dedicated tests are needed.

The second TVP mirror mostly experiences irradiation from low energetic neutrons, slowly accumulated over years of lifetime. At the end of life, a total energy deposition of 5 Mrad is expected in the window. In this experiment, we aim to get ≈1Mrad as this choice balances a reasonably high energy deposition with a manageable level of activation. There are two concerns regarding activation: 1) activation in the blue room (see discussion in previous sections), and 2) activation of the window which needs to be limited to safely examine the samples afterwards.

As the energy deposition that can be reached during the experiment is relatively low (maximum ≈0.4 Mrad), two options are investigated to obtain a higher energy deposition of ≈1 Mrad. First, the energy deposition and activation are analyzed when additional pulses are launched to the windows after the tungsten experiment has finished. Second, we briefly look at the possibilities with the ProNova [1] facility that can deliver a continuous beam of 50-200 MeV protons.

First, we discuss the neutron radiation around the tungsten blocks (steel shielding is not considered in the model). Second, we analyze the energy deposition in the windows. Third, we examine the activation of the windows. Fourth, we investigate the energy deposition and activation when additional pulses are used to increase the energy deposition. Fifth, we explore an alternative option at the ProNova facility. All these analyses are intended as an order-of-magnitude evaluation.

4.3.1 Neutron radiation around the tungsten blocks

With each pulse, the neutrons ejected by spallation reactions in the tungsten blocks create a radiation field around the tungsten blocks during the experiment. The dose from neutrons, accumulated from all pulses during the experiment, is shown in figure 38 and 39 for respectively a vertical and horizontal cut through the geometry. This dose, with units in Mrem, is the effective dose which considers radiation weighting factors for biological tissue. While this scaling is not appropriate for the (non-biological) window materials, the results still give an idea of the distribution of neutrons around the tungsten blocks. A more detailed look into the energy deposition in the window materials is discussed in the next section. These dose maps have been used to choose the initial location of the windows.

To have a closer look at the neutron spectra, the neutrons have been tallied as a function of their energy in five voided test disks above the middle tungsten block (see figure 40). The total neutron dose in these disks varies between 1 and 3.5 Mrem. Most of the neutrons coming out of the tungsten blocks have a high energy with the peak of the neutron energy distribution around 1 MeV (see figure 41), while the spectrum that we calculated at the location of the 2nd TVP mirror at the STS target (brown line) has much higher contributions from low energy neutrons.

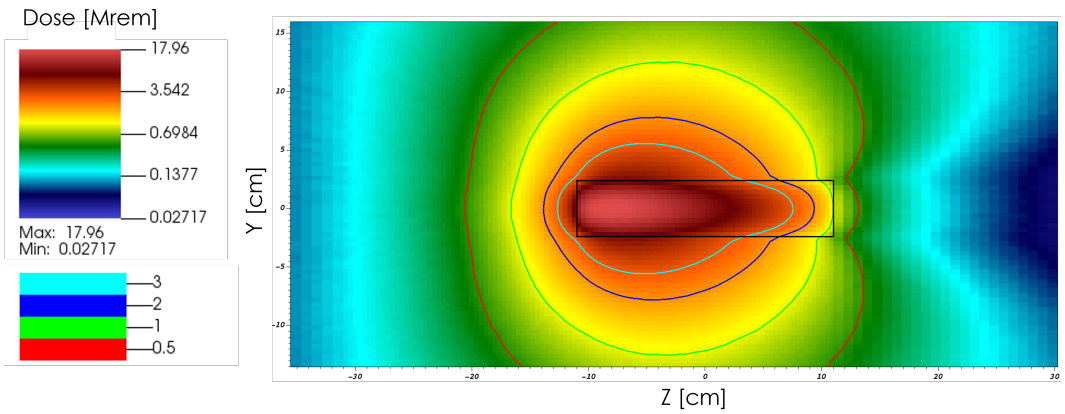

Figure 38. Total neutron dose [Mrem] accumulated during the experiment in a vertical cut through the middle of the tungsten block configuration (x=0cm))

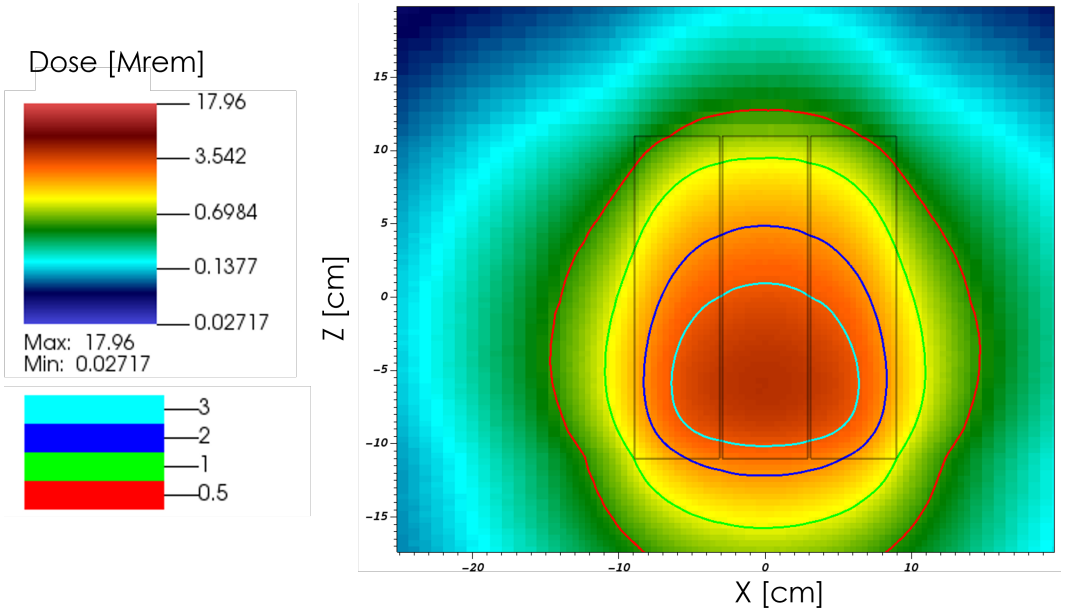

Figure 39. Total neutron dose [Mrem] accumulated during the experiment in a horizontal cut at y=3.8 cm, which is 1.4 cm above the tungsten surface.

For the windows irradiated in the Blue Room experiment, it has been checked that the dose from photons is more than 100 times lower than the dose from neutrons. This aspect is similar to the conditions at the 2nd TVP mirror.

Table 17. Total neutron dose [Mrem] for the test disks

Disk nr	Neutron Dose [Mrem]
1	3.49
2	2.06
3	1.00
4	3.09
5	2.25

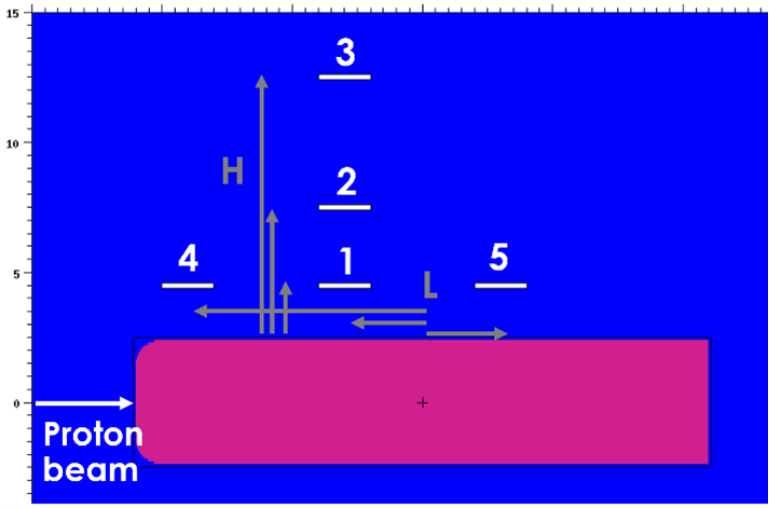

Figure 40. Location of the test disks for which the neutron and proton spectra are tallied

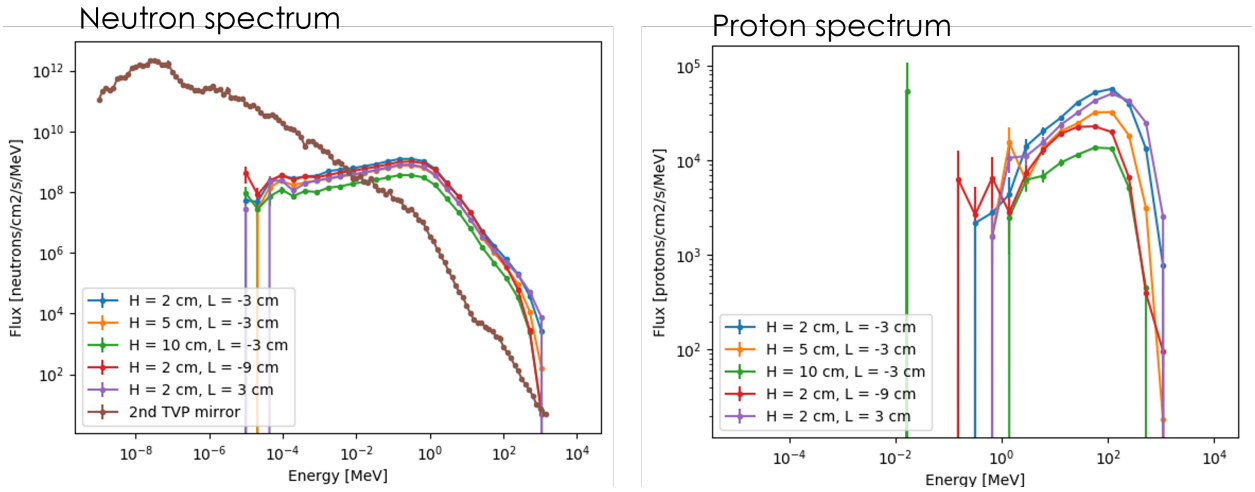

Figure 41. Neutron (left) and proton (right) flux as a function of energy [MeV] for the 2nd TVP mirror (brown, only in left graph) and the test disks above the tungsten configuration (all other colors).

4.3.2 Energy deposition in windows

The windows located below the tungsten blocks (numbered 1 to 10) receive approximately 0.1 Mrad (see figure 42 and 43). Windows 14 to 17, located behind the tungsten blocks, receive the highest doses of approximately 0.35 Mrad. Most of the deposited energy comes from the ionization paths of protons. Charged particles loose energy continuously when traveling through a material, while most neutrons pass through the material without any interaction. The windows with the highest energy deposition (14 to 17) are, therefore, located in the streaming path of the proton source. While the windows at the bottom see a neutron flux that is several orders of magnitude higher than the proton flux, ≈70% of the energy deposition originates from the ionization paths of protons. The remaining ≈30% is related to the interactions from neutrons and their secondary particles.

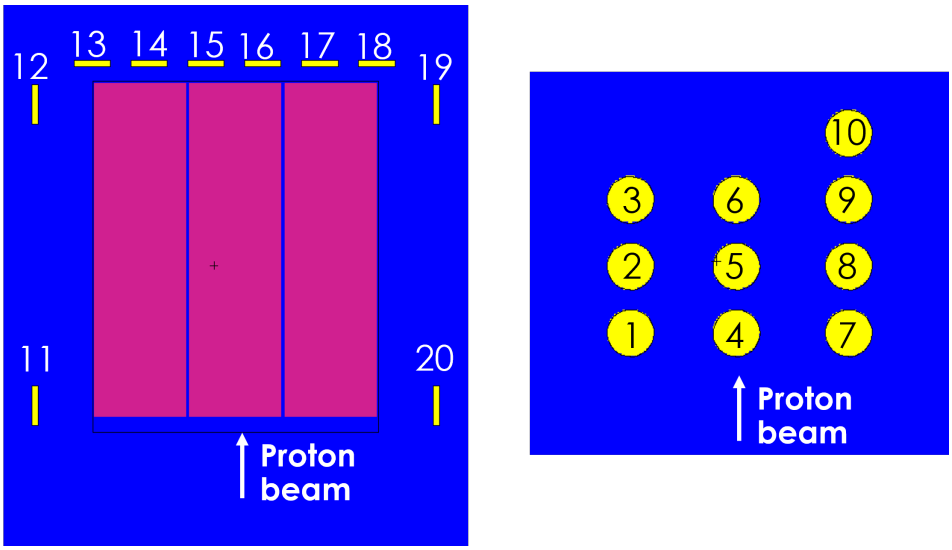

Figure 42. Position and numbering of the windows around the tungsten blocks. The right figure shows the windows located in a horizontal plane below the tungsten blocks.

The total energy deposition in the other considered window materials is up to 40% higher than in BaF2. The values for window nr. 4 at the bottom and window nr. 15 are listed in table 18.

Table 18. Energy deposition [Mrad] for all window materials for window number 4 and 15

	BaF2	ZnSe	ZnS	CaF2	Ge	MgF2	Sapphire (Al2O3)	Quartz (SiO2)	Fused Si (SiO2)
Nr. 4	0.134	0.138	0.161	0.189	0.137	0.185	0.186	0.187	0.188
Nr. 15	0.384	0.406	0.453	0.518	0.410	0.522	0.530	0.534	0.533

In general, the total energy deposition is considered a good measure regardless of the type of interaction causing it [10]. However, several differences need to be considered when comparing with the actual environment of the second TVP window:

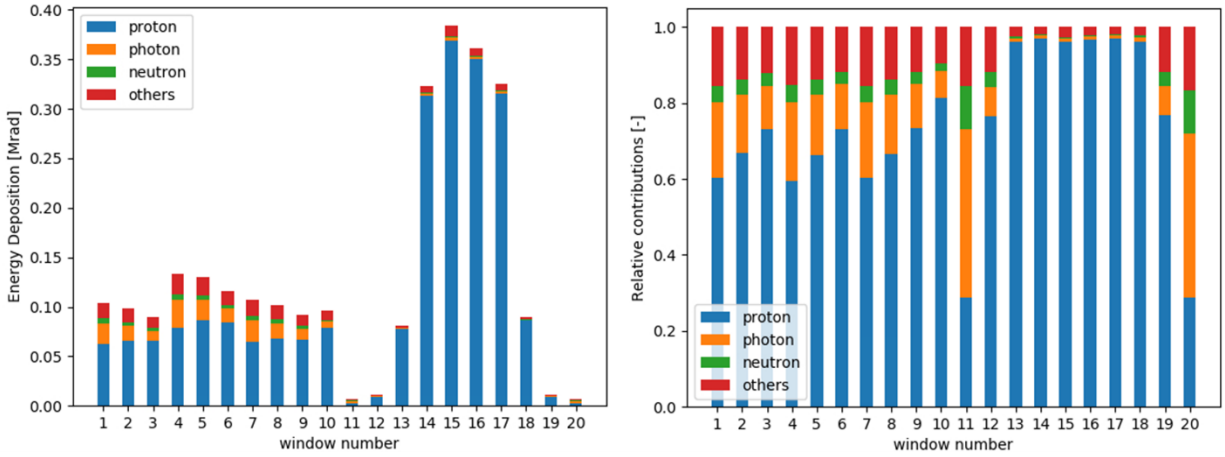

Figure 43. Energy deposition [Mrad] accumulated during the experiment in the 20 windows (all BaF2). Contributions of protons, photons, neutrons, and other particles are indicated in respectively blue, orange, green, and red.

- charged particles have a much higher energy deposition rate than neutral particles,
- the energy spectrum of the particles is much higher than what is expected in the real window environment,
- different transmutation products will occur,
- the energy deposition is delivered in short, intense pulses instead of at a slow, continuous rate.

While it is unclear how much the source of energy deposition influences the resulting damage in the material, it is expected that the resulting damage will give an indication in the right direction. The results of this experiment can be useful to decide which further investigation of the effects of radiation damage will be required.

4.3.3 Activation of the windows

The windows and their frames need to be handled hands-on for examination. Therefore, the activation should be limited. As a dose rate to aim for, we choose 10 mrem/h after 3 months.

The window and its frame consist of three different materials, which activate differently. This is clearly seen from the different source strength profiles in figure 44 and 45, which show respectively the source strength as a function of time for each of the parts of the window (here BaF2) and the frame (steel S304 and aluminum Al6061), and the dose rates in a plane located right next to the window and its frame are shown for several time steps. With only 1 hour decay time, the whole window configuration is highly active and dose rates reach ≈3.3 rem/h. After 1 day, the maximal dose rate decreases to 0.7 rem/h and the contribution from Na-24 in the Al6061 part of the frame becomes dominant. After 7 days and for longer decay times, the dominant contribution to the dose comes from activation of the steel, containing several major gamma emitters such as P-32, V-48, Sc-46, Mn-54 Co-56, Co-58, and Ti-44. After 3 months, a dose rate of 14 mrem/h is expected on the steel components. The approximate maximal dose rates are listed in table 19.

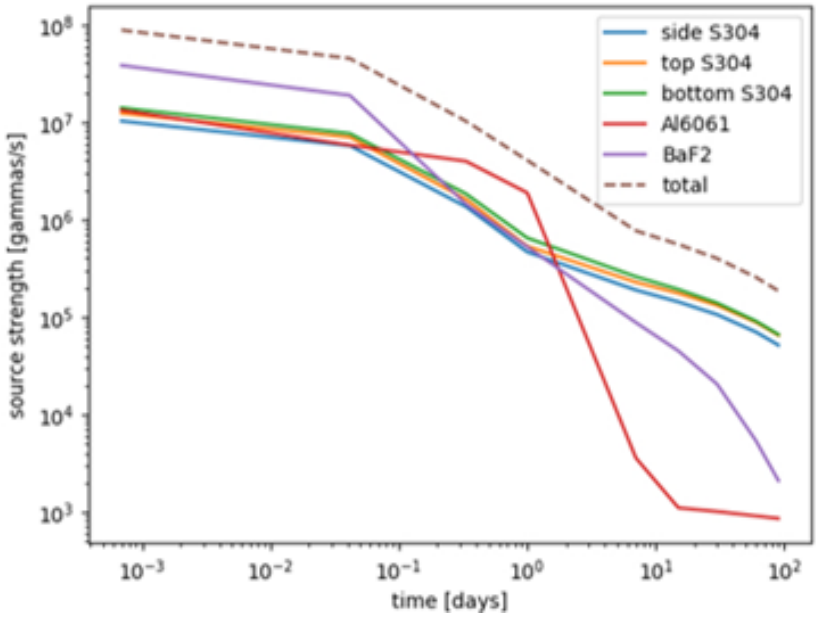

Figure 44. Activation source strength as a function of time for the different parts of the window (here BaF2) and its frame (S304 and Al6061)

To decrease the dose for longer decay times (weeks-months), it is suggested to replace the steel parts by aluminum. With a full Al6061 frame, the maximal dose rate after 3 months of decay time reduces to 0.26 mrem/h (and to 0.4 mrem/h considering aluminum with a high level of impurities, see table 19). The 10 mrem/h limit is reached after 15 days. At longer decay times (> 2 weeks), the main contributor to the dose

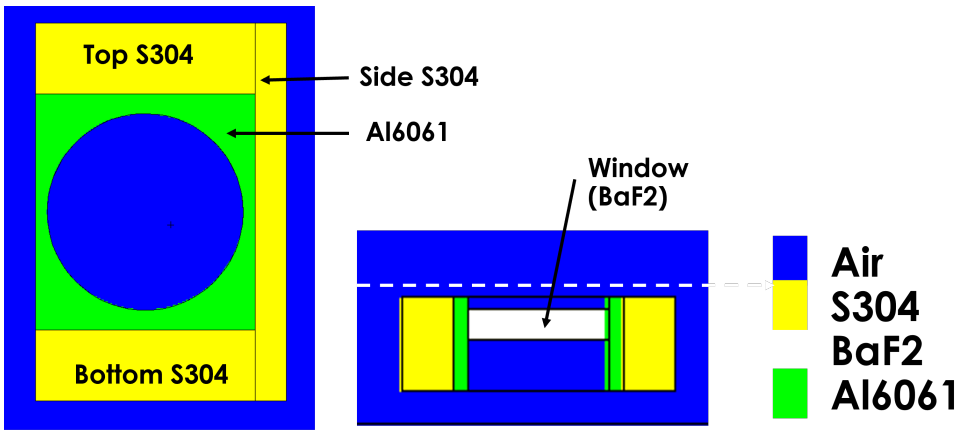

Figure 45. Representation of the model of the window and its frame. The dashed white line shows the plane at which the dose rates are shown in figure 46

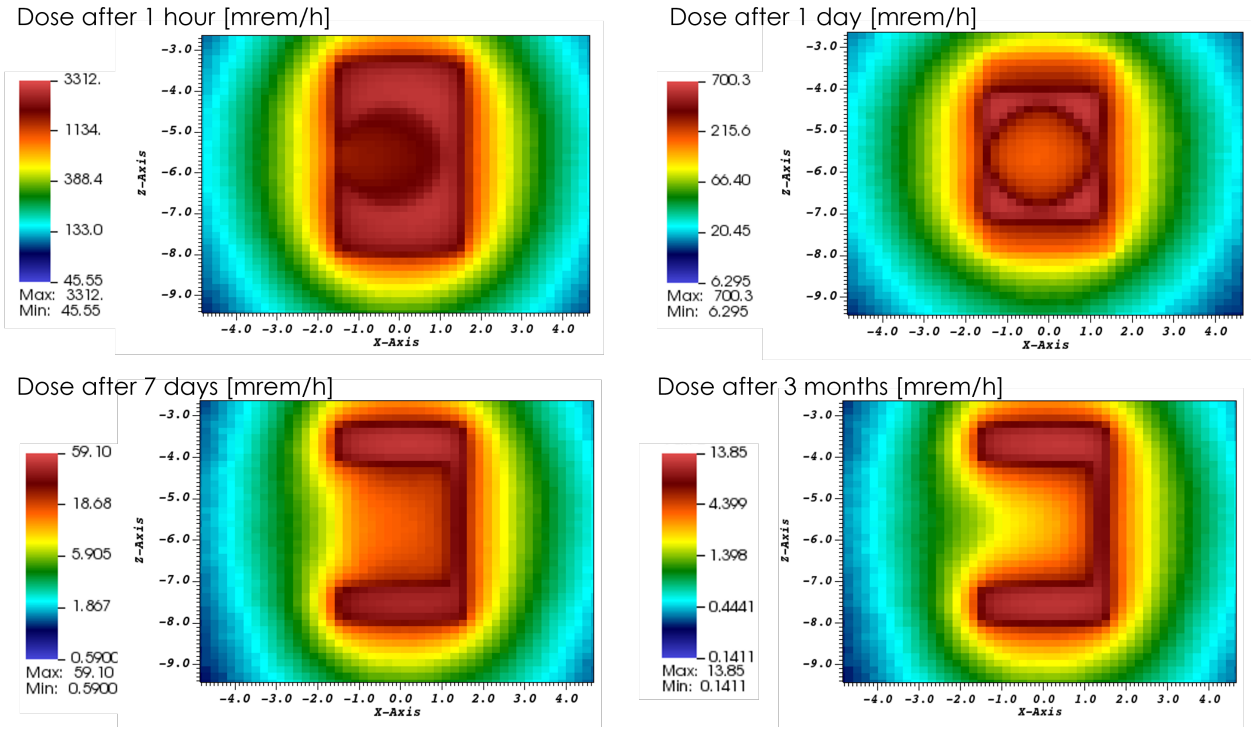

Figure 46. Dose rates [mrem/h] just above the window with its frame (Al6061 and S304) at several decay times. The dashed line in figure 45 illustrates the location of the plane in the geometry.

in activated aluminum is Na-22, with a half-life of 2.5 years. Its total amount is limited which results in a manageable dose rate.

Comparing the activation in other window materials to BaF2, windows in ZnSe, ZnS and Ge have higher source strengths for longer decay times (> 2 weeks), see figure 47 . Moreover, their energy spectra show higher contributions from high energy gammas than the energy spectrum of activated BaF2. A window

Table 19. Approximate maximal dose rates [mrem/h] as a function of time for frames with 3 different material compositions.

Indicator	Time	S304 and Al6061 frame	Al6061 frame	Al6061 frame with a high level of impurities
2	1 min	6.5e3	6.6e3	9.6e3
3	1 hour	3.3e3	3.3e3	4.4e3
4	8 hour	1.6e3	2.3e3	3.0e3
5	1 day	7.0e2	1.0e3	1.4e3
6	7 days	5.9e1	1.1e1	1.1e1
7	15 days	4.2e1	6.0e0	6.0e0
8	1 month	2.9e1	2.6e0	2.6e0
9	2 months	1.9e1	6.5e-1	7.0e-1
10	3 months	1.4e1	2.6e-1	4.0e-1

made from ZnSe, ZnS and Ge is expected to become a similar contributor to the dose as the steel parts of the frame. Further calculations are necessary to obtain more accurate estimates for the dose rates.

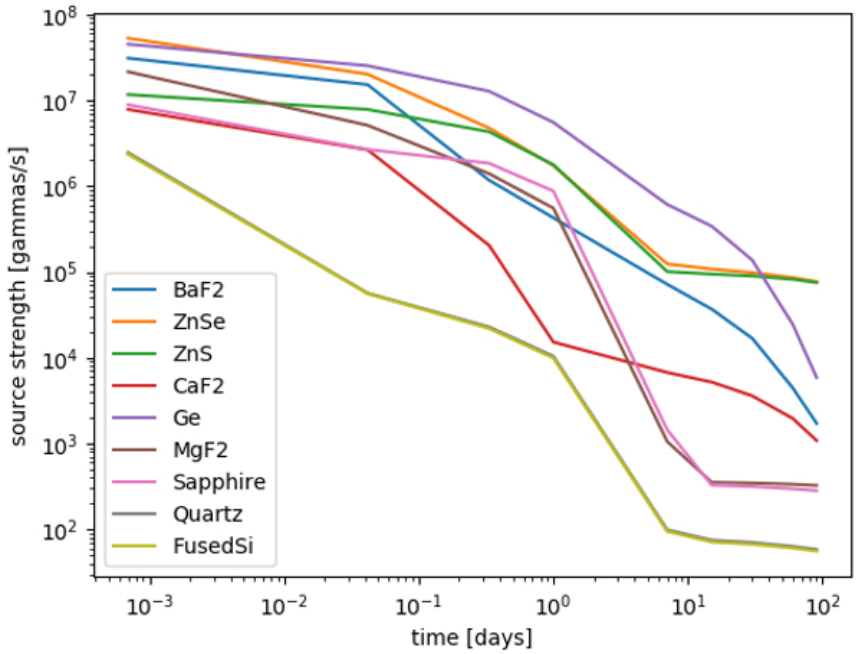

Figure 47. Activation source strength [gammas/s] in the window for all window materials

4.3.4 Additional pulses: energy deposition and activation

Because only 0.1-0.4 Mrad can be reached in the windows around the tungsten blocks during the experiment, it is considered to use additional pulses impinging directly on a window after the tungsten experiment to increase the total energy deposition. Per full intensity pulse (3e13 protons), ≈0.1 Mrad can be reached (see table 20). This means that only 10 pulses are needed to reach ≈1 Mrad.

Table 20. Energy deposition per proton pulse (3e13 protons, gaussian distribution with a standard deviation of 1 cm) in 4 window materials

Window material	Total energy deposition per pulse [Mrad]
BaF2	0.106
ZnSe	0.113
ZnS	0.122
CaF2	0.134

The 10 additional pulses will activate the tungsten configuration (no cladding assumed) and steel shielding further. These pulses are received with the front shielding closed. The windows will be attached to this front shielding. Just one window (BaF2) in its frame (S304 and Al6061) are considered for this analysis. The highest activation source comes from the tungsten, especially the middle block which receives most protons. The carbon steel shielding around will also get highly activated, not only from the protons passing through the front shielding, but also from the neutrons produced in the tungsten blocks. A smaller activation source comes from the window itself. The resulting dose rates after 1 hour and 8 hours of decay time are shown in figure 48 and 49 for a horizontal cut through the middle of the geometry (both figures have the same scale). While the middle tungsten block gets highly activated, it is shielded well by the steel. The activated steel gives the highest contribution to the dose in the room, especially the front part. Therefore, higher dose rates are present in the front of the configuration than on the sides and at the back. The window itself has a smaller, more local effect due to its small volume.

The dose rates at the detectors 30 cm from the steel shielding after 1 hour of decay time range from 13 at the back to 85 mrem/h at the front (see figure 50 and table 21). These values are only the contributions to the dose of 10 additional pulses. To obtain the total dose rate, these values need to be added to the dose rates previously calculated from the tungsten experiment. Without much decay time between the experiment and the additional pulses, dose rates can reach 100 mrem/h in front and at the top. Additional pulses highly increase the dose in the front section of the configuration. If a person is entering the room, this section should be avoided. As the main contribution to the dose comes from Mn-56 in the activated steel, the difference in dose between 1h and 8h of decay time is large. Waiting longer before entering the room is, therefore, an excellent strategy to limit exposure.

The dose rates of the window in its frame are calculated to ensure they can be handled hands-on for examination. Indeed, a dose rate below 10 mrem/h is reached after 1 to 2 months (see table 22).

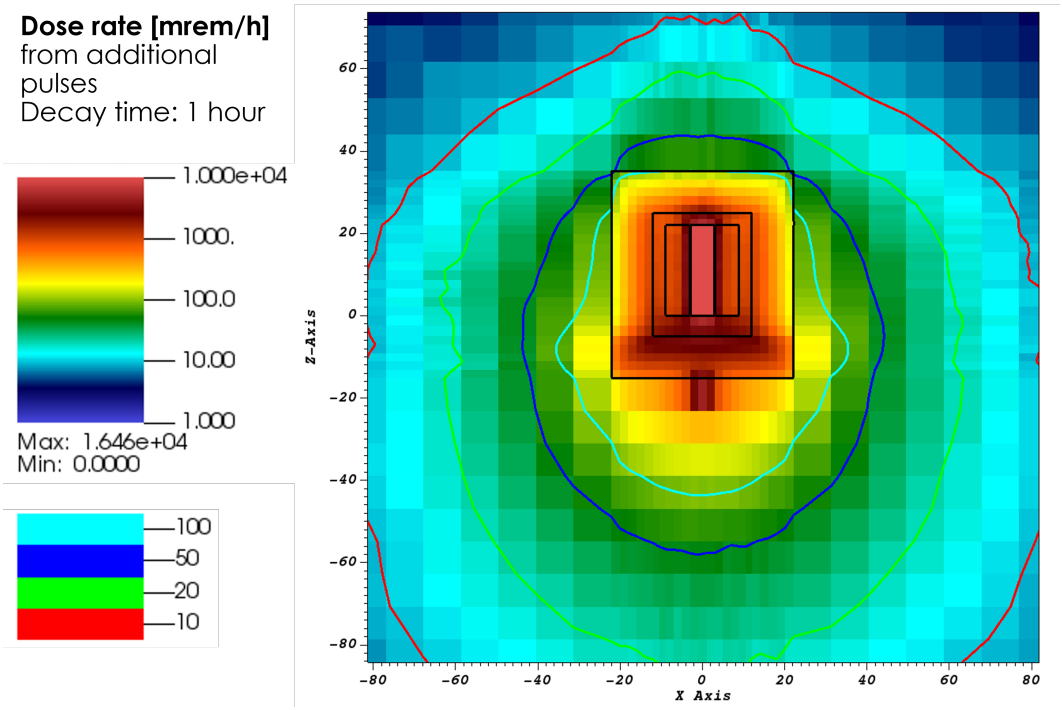

Figure 48. Dose rate [mrem/h] from additional pulses after 1 hour of decay time in a horizontal cut through the middle of the geometry

Table 21. Dose rates [mrem/h] from additional pulses at detector points 30 cm from the steel.

	Left	Top	Front	Back
After 1h	27	41	85	13
After 8h	3.3	4.9	10	1.5

Table 22. Approximate maximal dose rates [mrem/h] of the window and its frame (S304 and Al6061) for several decay times.

indicator	Time	Approximate max dose rate [mrem/h]
2	1 min	2.1e5
3	1 hour	2.9e4
4	8 hour	2.4e3
5	1 day	4.6e2
6	7 days	6.3e1
7	15 days	2.6e1
8	1 month	1.1e1
9	2 months	5e0
10	3 months	3e0
11	6 months	1.3e0
12	9 months	7e-1
13	1 year	5e-1

Considering other window materials, higher dose rates are expected for ZnSe, ZnS and Ge. The source

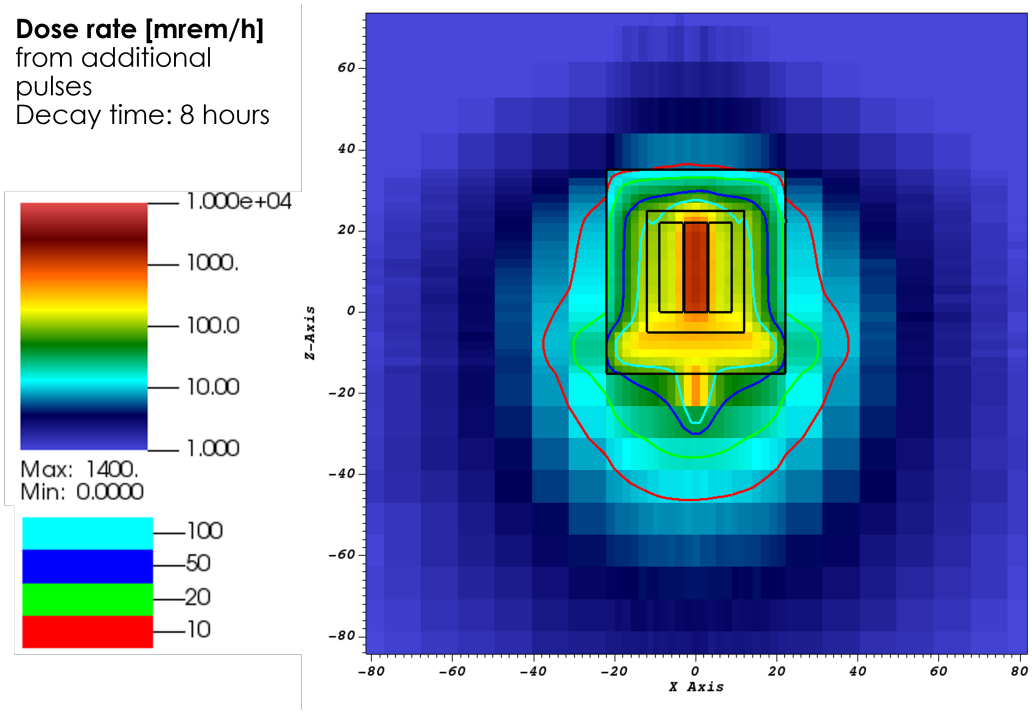

Figure 49. Dose rate [mrem/h] from additional pulses after 8 hours of decay time in a horizontal cut through the middle of the geometry

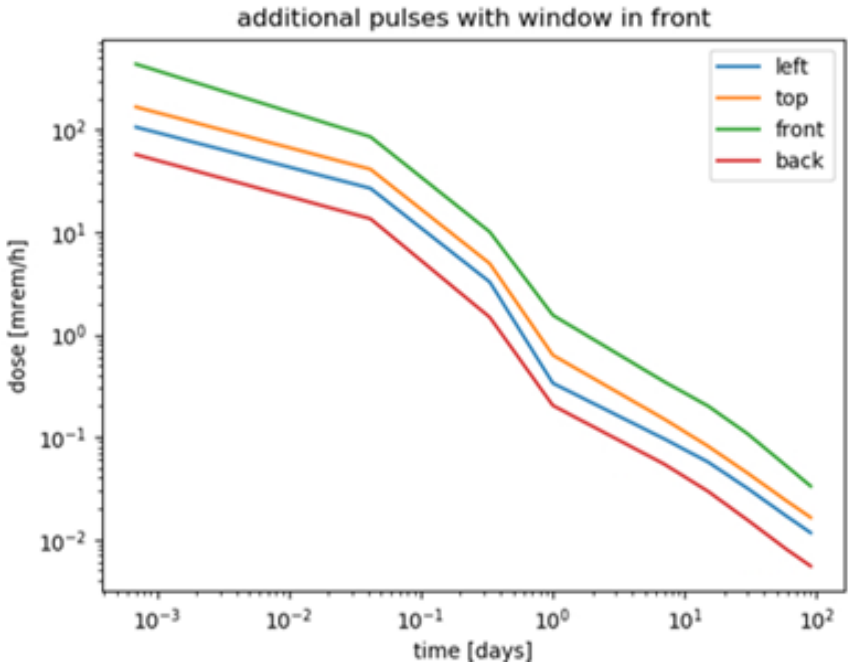

Figure 50. : Dose rates [mrem/h] at detectors 30 cm from the steel shielding These dose rates only consider the activation from the additional pulses, not the pulse series of the tungsten experiment.

strengths for the window materials are shown in figure 51. A similar discussion as in the previous section applies. Further calculations are required for accurate dose estimates.

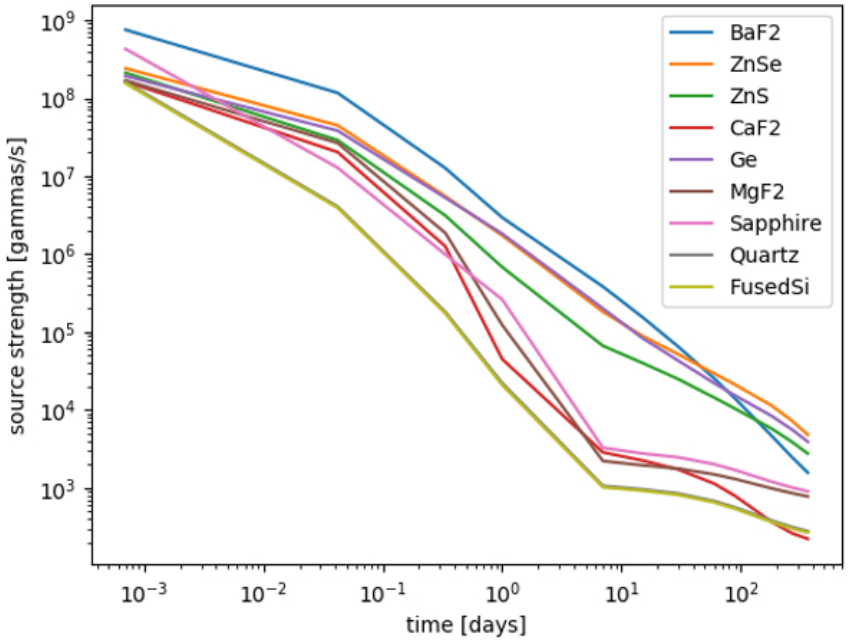

Figure 51. Activation source strength [gammas/s] in the window for all window materials for the additional pulses.

4.3.5 Alternative window irradiation experiment at ProNova

The ProNova Radiation effects testing facility [1] at CARES Proton Therapy Knoxville has a dedicated beam line for proton testing. It can provide a continuous beam of maximum 5.5 nA of 200 MeV protons. The minimum proton energy is 50 MeV. The continuous delivery of protons (instead of pulses) with a lower energy provides an advantage over the blue room experiment for testing window materials. Additionally, there is less concern about activation in the room without the tungsten configuration present. In this section, we evaluate the time to reach 1 Mrad in each window material with a simple estimate.

Most of the energy deposition from protons comes from electromagnetic interactions producing ionization along the proton path and is tabulated in, for example, the SRIM database as the stopping power dE/dx, with E the energy and x the distance. The energy deposition in Rad/s is calculated as follows:

$$S\left[\frac{Rad}{s}\right] = \frac{dE}{dx}\left[\frac{MeV}{mg/cm^2}\right] * I\left[\frac{1}{s}\right] * \frac{1}{A[cm^2]} * 1.6 * 10^{-5}\left[\frac{Rad}{MeV/mg}\right] \quad (2)$$

With I the number of protons per second (5.5 nA = 5.5e-9/1.6e-19 protons/s = 3.43255e10 protons/s), and A the surface area of the window with a 1.25 cm radius. This assumes that all protons are interacting with the window. Table 23 lists the stopping powers dE/dx from SRIM [9], the energy depositions in rad/s, and the number of hours that is required to reach 1 Mrad for all considered window materials for 50 MeV and 200 MeV protons. With 50 MeV protons only 15-20 mins are needed to reach 1 Mrad. With 200 MeV protons (that have a smaller stopping power) it takes 40-55 mins to reach 1 Mrad.

Table 23. Estimate for the number of hours to reach 1 Mrad based on the ionization energy deposition dE/dx [MeV/(mg/cm2)] for 50 MeV and 200 MeV protons.

	dE/dx 50 MeV	dE/dx 200 MeV	rad/s 50 MeV	rad/s 200 MeV	hours to 1 Mrad 50 MeVd	hours to 1 Mrad 200 MeV
SiO2	1.04E-02	3.80E-03	1,167.24	425.52	0.24	0.65
BaF2	7.38E-03	2.79E-03	827.61	312.72	0.34	0.89
ZnSe	7.77E-03	2.93E-03	871.11	328.19	0.32	0.85
ZnS	8.63E-03	3.22E-03	967.65	361.27	0.29	0.77
CaF2	9.84E-03	3.61E-03	1,102.76	404.55	0.25	0.69
Ge	7.78E-03	2.93E-03	871.90	328.42	0.32	0.85
MgF2	9.99E-03	3.65E-03	1,120.59	408.93	0.25	0.68
Sapphire	1.02E-02	3.72E-03	1,143.69	417.22	0.24	0.67

A quick MCNP simulation confirms the results. For a 4mm thick window and a uniformly distributed proton source over a cylindrical surface with a radius of 1.25 cm (same as the window surface area), the energy deposition is calculated for a SiO2 and BaF2 window, with respectively densities of 2.32 g/cm3 and 4.89 g/cm3. The results for several proton energies are listed in table 24, and are very similar to the quick estimates based on dE/dx.

Using protons, it could be considered to create a source of neutrons, such that the energy deposition resembles the conditions at the 2nd TVP window more closely. With neutrons, however, it takes a much longer time to accumulate a relevant amount of energy deposition. Charged particles, such as protons, are very advantageous to accumulate large amounts of energy deposition in a short time. Protons and other

Table 24. Estimate for the number of hours to reach 1 Mrad based on MCNP simulations for Si02 and BaF2.

Proton energy [MeV]	Hours to 1 Mrad for SiO2	Hours to 1 Mrad for BaF2
50	0.22	0.30
100	0.39	0.55
150	0.51	0.71
200	0.64	0.88

charged particles continuously lose energy along their track, while neutrons mostly pass the material without interacting. This results in 100-1000 times higher energy losses with protons than with neutrons. This is demonstrated by a simple MCNP calculation in which the proton source is replaced by a neutrons source with the same flux. In table 25, we list the total energy deposition and its contributions from protons, neutrons, and photons/electrons (mostly generated by neutron interactions) for a BaF2 window. We also list the number of hours to reach 1 Mrad, which gives an easier to interpret measure of the difference. With 50 MeV neutrons instead of 50 MeV protons, the energy deposition drops by 2 orders of magnitude: it takes 46.6 hours to reach 1 Mrad. Most neutrons created in a spallation reaction will have a lower energy, which also results in less energy deposition: with 1 and 0.1 MeV neutrons, it takes 722 to 1095 hours to reach 1 Mrad. Keeping these orders of magnitude in mind, it seems unreasonable to create a neutron source that can create enough damage in a reasonable time.

Table 25. Comparison of energy deposition between protons and neutrons for a BaF2 window. All simulations assume 3.43255e10 particles/s. The total energy deposition includes protons, neutrons, photons, electrons and secondary particles. As the contribution of the secondary particles is not listed, the total can be larger than the sum of the listed contributions.

	Total energy deposition [MeV/g/s]	Energy deposition from protons [MeV/g/s]	Energy deposition from neutrons [MeV/g/s]	Energy deposition from photons and electrons [MeV/g/s]	Hours to 1 Mrad
50 MeV protons	5.77e10	5.75e10	6.5e5	1.38e7	0.3
50 MeV neutrons	3.72e8	1.13e8	8.62e7	1.3e7	46.6
1 MeV neutrons	2.41e7	0	6.76e6	1.7e7	722
0.1 MeV neutrons	1.59e7	0	7.35e5	1.51e7	1095

The activation source strength for each window material accumulated during 30 minutes with 50 MeV protons (sufficient to reach 1 Mrad) are generally similar in magnitude to those obtained with the 800 MeV proton pulses (see figure 52). More detailed analysis is needed to obtain accurate dose rate estimates.

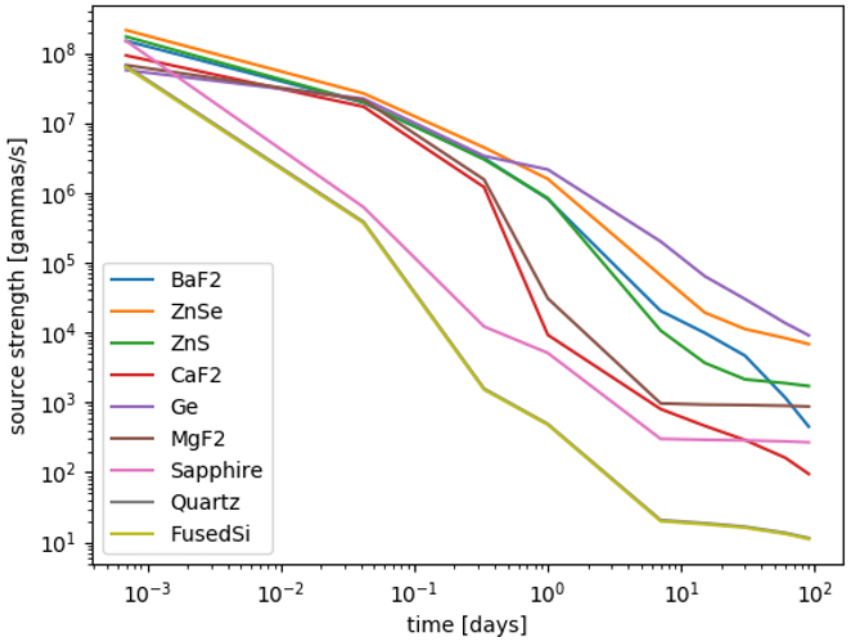

Figure 52. Activation source strengths in the window materials for 30 mins of irradiation with 50 MeV protons (3.43255e10 protons/s).

5 CONCLUSIONS

The energy deposition has been calculated for the three lay-outs considered in the Blue Room Experiment. For protons at 800 MeV, the energy deposition profile in the tungsten block shows a small local increase at ≈21 cm followed by a sudden decrease to a negligible value because the protons range out. This effect is highly dependent on the proton energy and could lead to additional undesired internal stresses with lower proton energies. With STS-like conditions (protons of 1.3 GeV), the protons go all the way through the target and do not generate a Bragg peak. Several 3-block tungsten configurations have been considered and analyzed in the preparation of this experiment. They differ in the presence of Ta-clad on one of the blocks and in small geometric features such as roundings. Additionally, several beam sizes and positions have been investigated, as the energy deposition profile and its maximum are highly dependent on the beam characteristics. Files detailing the energy deposition in the blocks have been made available for thermal and stress analysis.

The tungsten blocks will be activated after the experiment. Dose rates have been calculated with a simplified and high-fidelity simulation approach. If the room needs to be cleared within one day after the experiment, actions should be taken to reduce exposure to people entering the room. A 4-inch carbon steel shielding on all the sides efficiently reduces the dose from the activated tungsten. However, carbon steel itself becomes highly activated itself if it is present during the experiment. Because of the 2.5 hour half-life of the dominant radioactive isotope (Mn-56), dose rates drop drastically after 8 hours to 1 day. The easiest way to reduce the dose rates in the room after the experiment is, therefore, to wait longer before entering the room. Activation of other structures/materials that might be present in the Blue Room have not been evaluated (as we do not have the information) but may contribute significantly to the dose rates in the room. To reduce radiation exposure from activation as much as possible after the experiment, additional shielding can be placed in the room after the experiment. Significant reductions in dose rates can be obtained by using a lead blanket over the tungsten/steel configuration or by adding a lead brick wall in the room. Additionally, a few alternative shielding materials have been explored. Lead shielding will result in lower dose rates, while aluminum shielding is not recommended.

If samples of windows are placed around the tungsten blocks, an energy deposition of 0.1-0.4 Mrad can be reached. As most neutrons pass the windows without interacting, the dominant contribution comes from ionization paths of protons. A total energy deposition of at least 1 Mrad is preferred and can be reached by using additional proton pulses impinging directly on the windows. This, however, will cause additional activation of the tungsten-steel configuration. An alternative is to use a proton beam in another facility such as ProNova, at which 1 Mrad can be reached within 1 hour. To examine the windows after irradiation, hands-on handling is required. A dose rate of 10 mrem/h can be reached within 1 to 3 months.

6 REFERENCES

[1] "Pronova." https://provisionhealthcare.com/locations-2/knoxville/rad-effects/, accessed 2021/11/15.

[2] R. M. Jr, C. Gesh, R. Pagh, R. Rucker, and R. W. III, *Compendium of Material Composition Data for Radiation Transport Modeling, Revision 1, Pacific Northwest National Laboratory, PIET-43741-TM-963, PNNL-15870 Rev. 1,*. 2011.

[3] C. Werner *et al.*, *MCNP User's Manual, Code Version 6.2, Los Alamos National Laboratory, LA-UR-17-29981*.

[4] S. T. Holloway, W. B. Wilson, C. T. Kelsey, H. Little, and V. Mozin, *A Manual of CINDER2008 Codes and Data, Los Alamos National Laboratory, LA-UR 11-00006*. 2011.

[5] I. I. Popova, *An Updated Manual for CINDER2008 Codes and Data in the AARE Package, Oak Ridge National Laboratory, ORNL/TM-2018/926*. 2018.

[6] W. Lu and F. X. Gallmeier, *Patching EAF-2010 into CINDER2008 Cross Section Libraries, Oak Ridge National Laboratory, ORNL/TM-2018/16*. 2016.

[7] I. I. Popova, *Flux to dose conversion factors,Oak Ridge National Laboratory, SNS-NFDD-NSC-TR-0001, R02*. 2012.

[8] "Plansee." https://www.plansee.com/en/materials/tungsten.html, 2021.

[9] J. F. Ziegler, J. Biersack, and M. D. Ziegler, "SRIM 2008.04." https://www.srim.org, 2008.

[10] R. E. Stoller, "1.13 - radiation damage correlation," in *Comprehensive Nuclear Materials (Second Edition)* (R. J. Konings and R. E. Stoller, eds.), pp. 456–467, Oxford: Elsevier, second edition ed., 2020.

APPENDIX A. COMPUTER HARDWARE AND SOFTWARE

APPENDIX A. COMPUTER HARDWARE AND SOFTWARE

The mcnp module loaded on saturn for energy deposition analysis and the calculation of dose rates is mcnp/mcnp6.2-intel19.1.3. For the calculations of the spallation products and neutron fluxes for the activation analysis module mcnp/mcnp6.2rnucs is used. The activation analysis itself uses module cinder/2008 on saturn. Attila4MC is used on a windows machine (Attila version 10.2.0.5388-beta3).

APPENDIX B. LOCATION OF COMPUTATIONAL INPUT AND OUTPUT FILES

APPENDIX B. LOCATION OF COMPUTATIONAL INPUT AND OUTPUT FILES

Input- and output-files can be found on the sts archive on saturn:
/home/sts_archive/S.07_R_D/Blue_Room. In this directory, there are 4 subdirectories:
energy_deposition_tungsten, activation_tungsten, activation_shielding, window_irradiation. These folders contain input and output files (for MCNP and AARE), python scripts used for analysis, text files that have been shared with Tom McManamy for stress analysis.

APPENDIX C. DETAILED FIGURES OF THE ENERGY DEPOSITION

APPENDIX C. DETAILED FIGURES OF THE ENERGY DEPOSITION

In figures 53, 54 and 55, we show the energy deposition [J/cc] and the relative error [-] for a vertical and horizontal cut through the geometry of the simple tungsten block (section 3.1.1) with a nominal beam (σ = 1 cm) directed to the center of the block, the edge of the block, and inbetween the gap with two blocks side by side. Similar graphs with a squeezed beam profile are shown in figures 56, 57 and 58. In figure 59 and 60, we show the energy deposition [MeV/g] with the simplified 3-block configuration (section 3.1.3) with a beam with σ = 6 mm directed towards the center of the middle block.

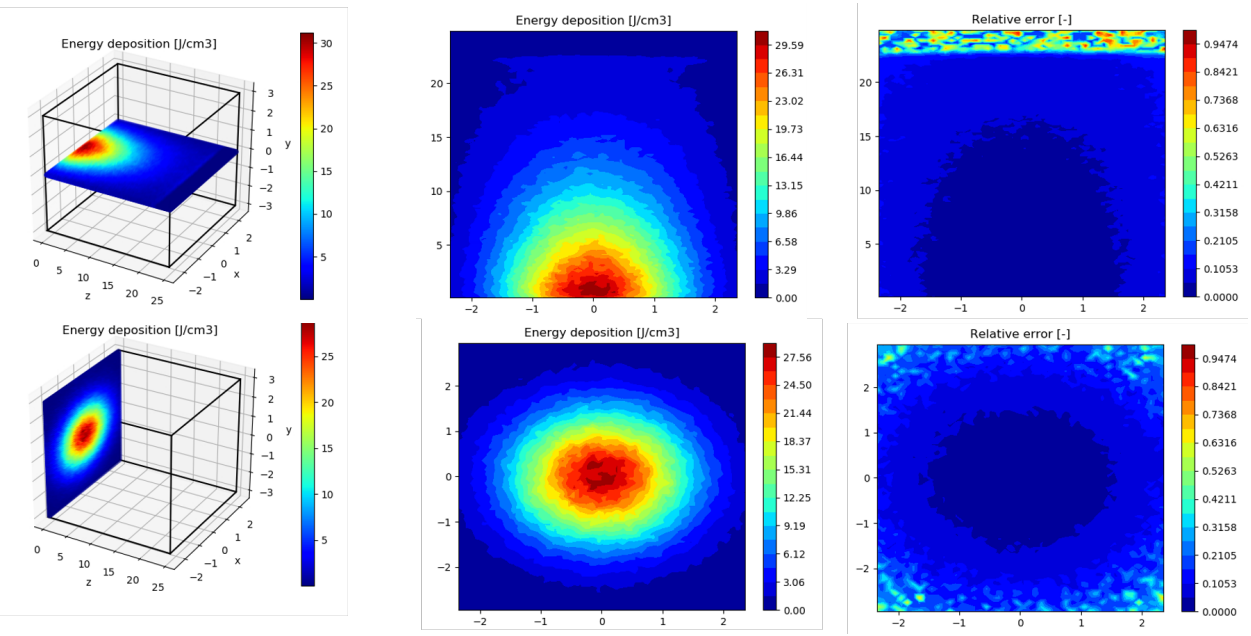

Figure 53. Energy deposition and relative error for two cross-sections in the tungsten block with the 'beam on center' layout with nominal beam.

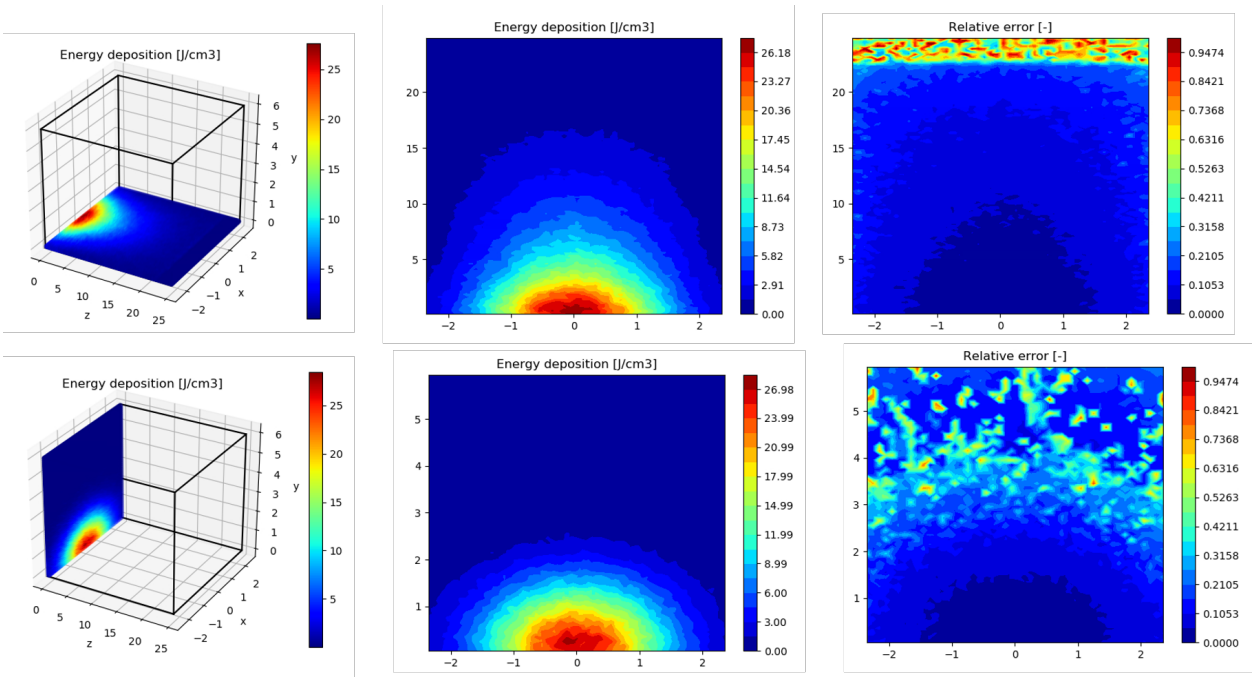

Figure 54. Energy deposition and relative error for two cross-sections in the tungsten block with the 'beam on edge' layout with nominal beam.

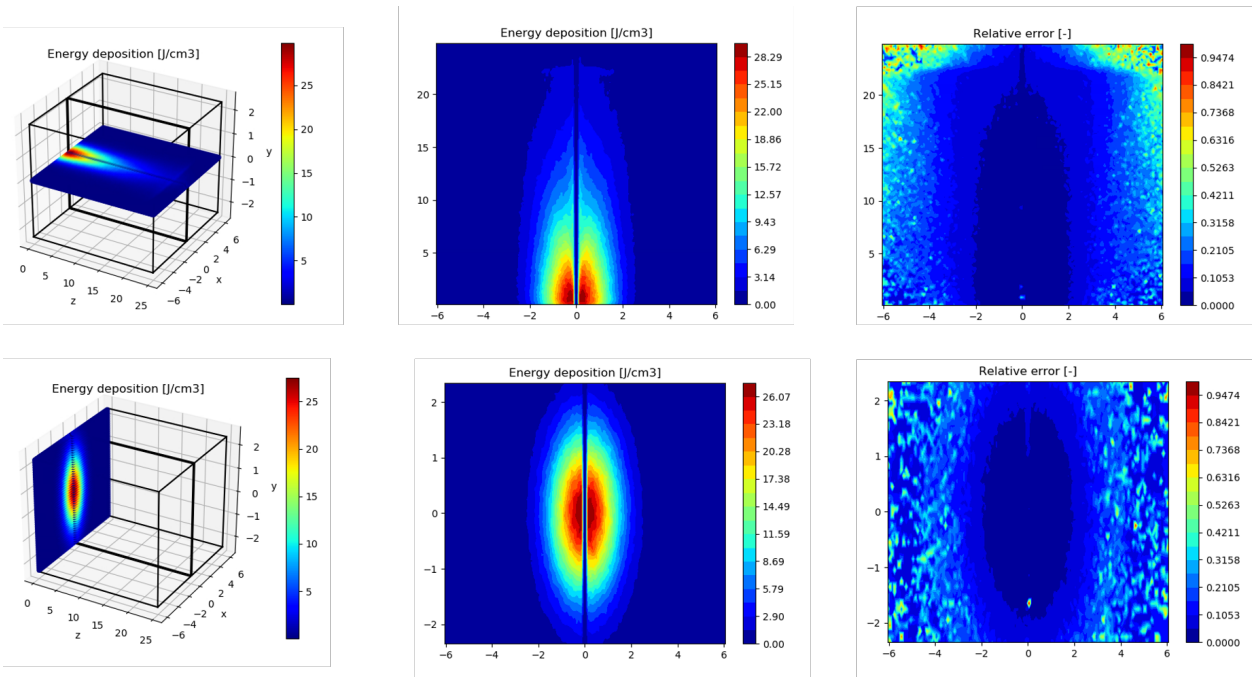

Figure 55. Energy deposition and relative error for two cross-sections in the tungsten block with the '2 targets side by side' layout with nominal beam

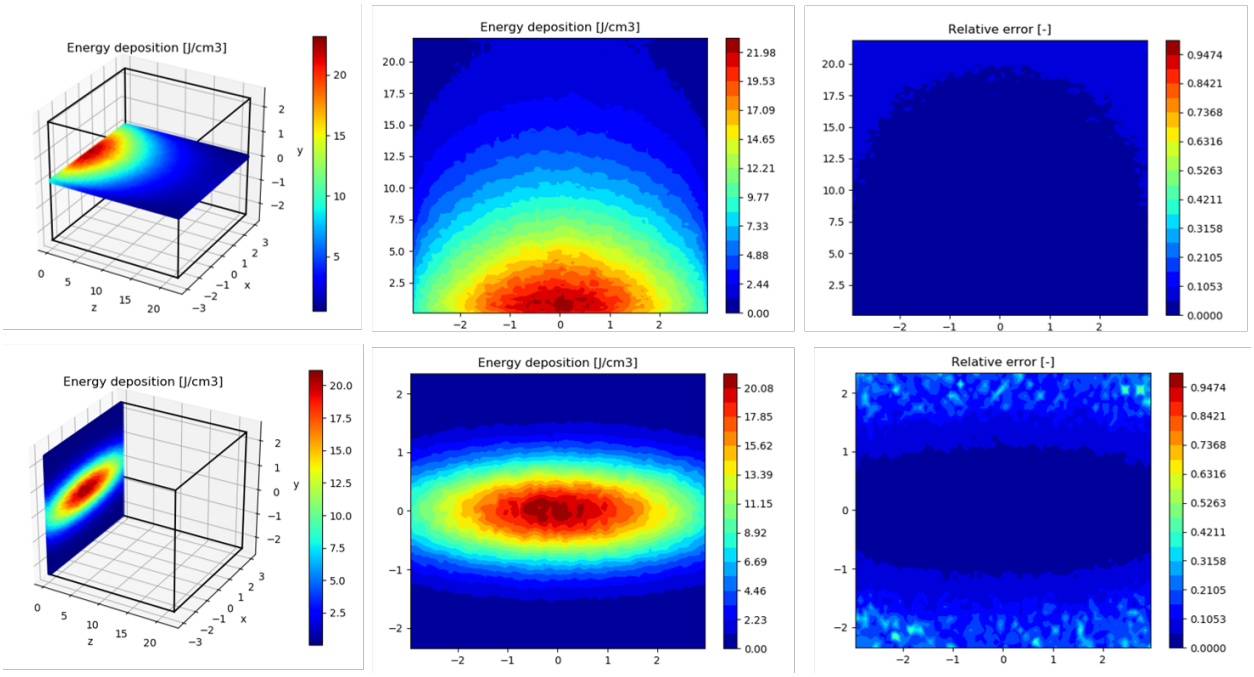

Figure 56. Energy deposition and relative error for two cross-sections in the tungsten block with the 'beam on center' layout with squeezed beam.

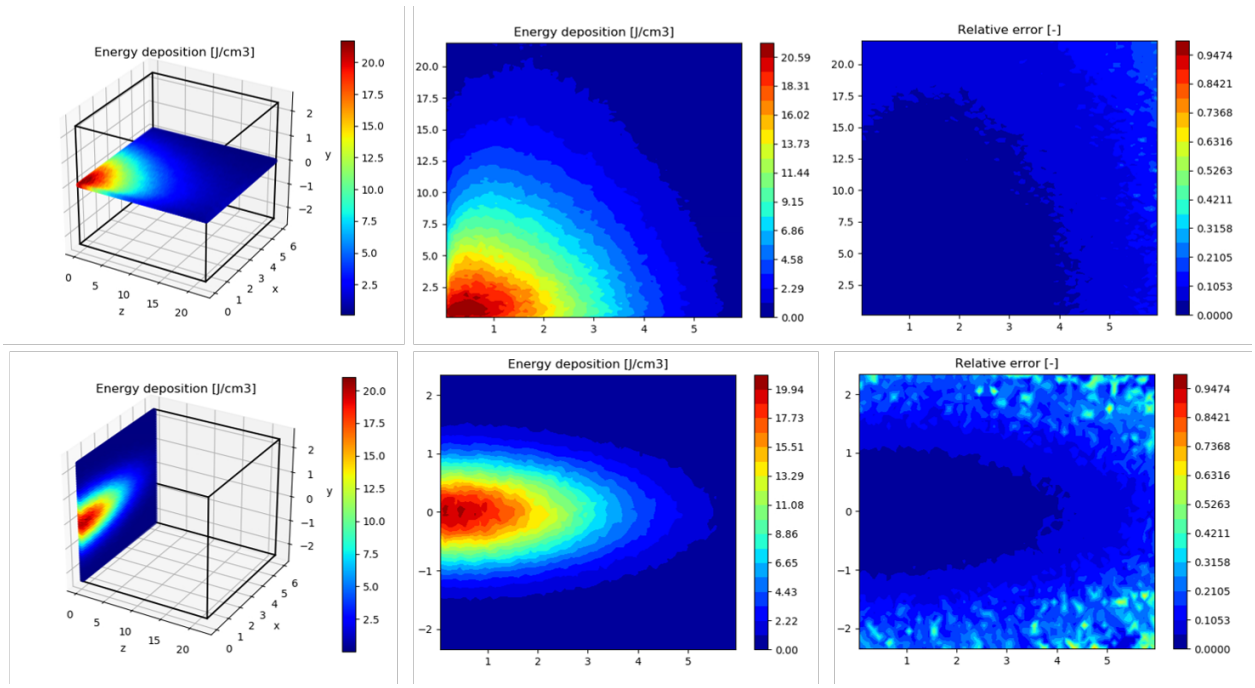

Figure 57. Energy deposition and relative error for two cross-sections in the tungsten block with the 'beam on edge' layout with squeezed beam.

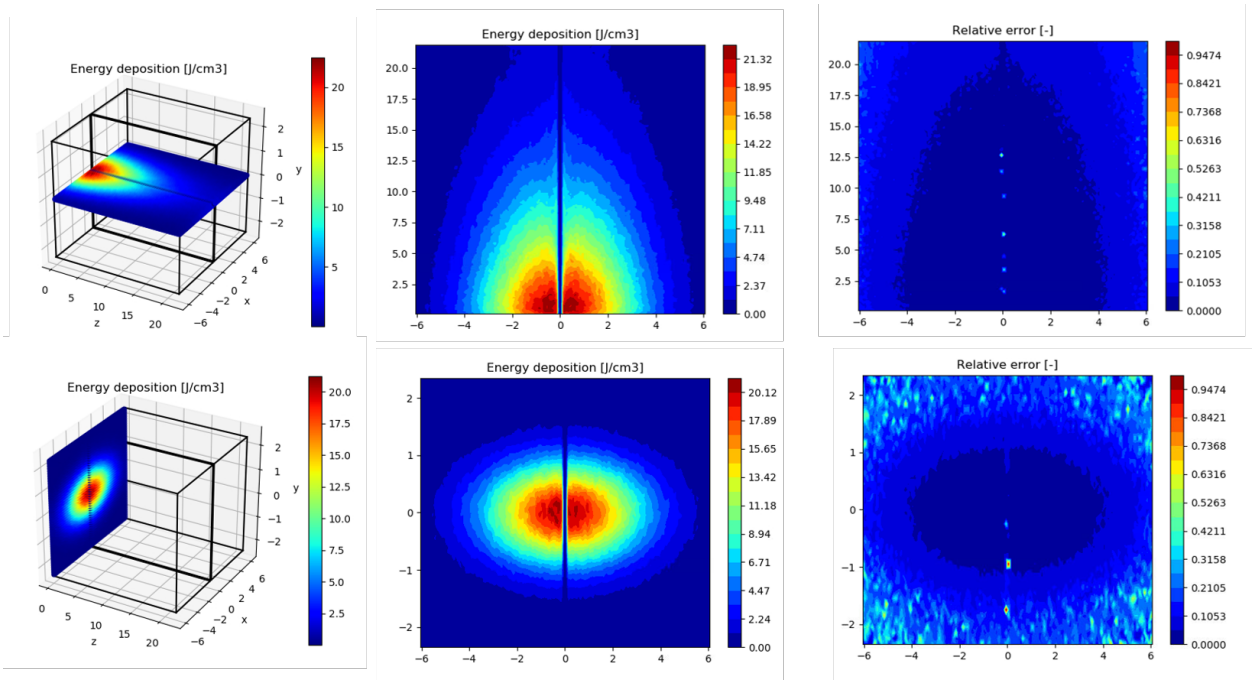

Figure 58. Energy deposition and relative error for two cross-sections in the tungsten block with the '2 targets side by side' layout with squeezed beam.

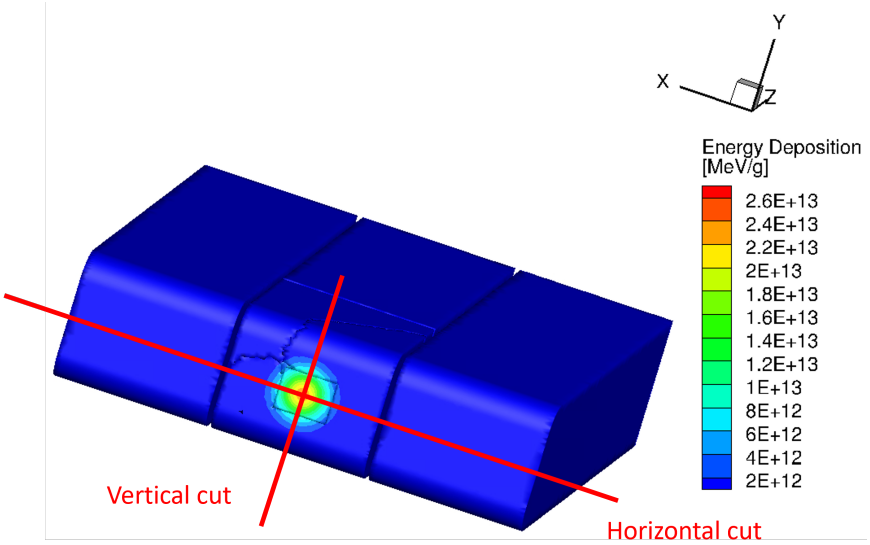

Figure 59. Energy deposition in the simplified 3-block configuration with a 6mm sigma.

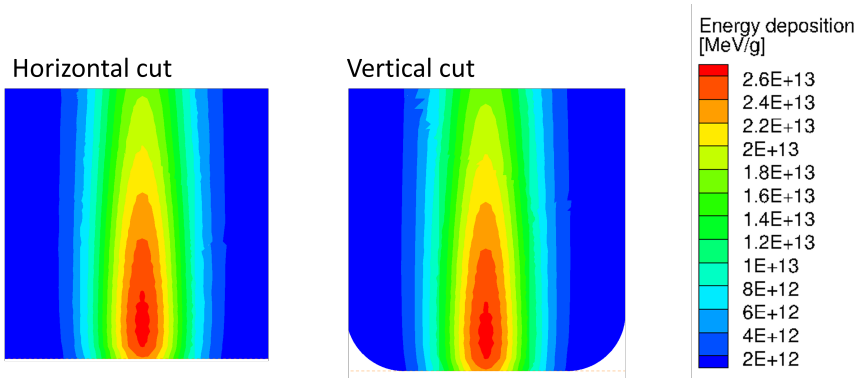

Figure 60. Energy deposition in a horizontal and vertical cut through the center of the middle block of the simplified 3-block configuration with a 6mm sigma.

APPENDIX D. EXPLORATION OF COMBINATIONS OF LEAD AND STEEL SHIELDING

APPENDIX D. EXPLORATION OF COMBINATIONS OF LEAD AND STEEL SHIELDING

The goal of this study is to explore shielding options that combine lead and steel such that the dose rates from the activated shielding are low, while keeping the total weight of the shielding limited.

Lead is a better shielding material than steel and it activates less (see section 4.10), but it also weighs more. With a combination of steel and lead, we hope to get some of the benefits of lead while having a smaller total weight.

Dose rate results for several configurations are summarized in table 13. The dose rates after 1 hour of decay are listed for detectors at 30 cm from the tungsten block, which is at a much closer distance to the shielding. Absolute values are, therefore, not that useful (and about 2x as high as for the detectors at 30 cm from the shielding), but the comparisons between the shielding materials is valid. These dose rates are only from the activated shielding itself and not from the activated tungsten inside. The contribution of tungsten, is however, much lower.

Table 26. Comparison of dose rates [mrem/h] after 1 hour for several shielding combinations of lead and steel. (MCNP errors <5%)

	Side	**Top**	**Back**
Steel 10 cm	100	130	91
Lead 10 cm	22	27	57
Steel 6 cm + lead 2 cm	50	70	76
Lead 2cm + steel 6 cm	110	150	100
Steel 4 cm + lead 2 cm	55	80	74